Crystallisation pathways of a mixed La-Nd carbonate – Ambient temperature synthesis of the mineral lanthanite

Journal Pre-proof

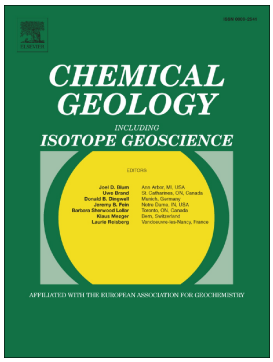

Crystallisation pathways of a mixed La-Nd carbonate – Ambient temperature synthesis of the mineral lanthanite

Dylan L. Price, Ian B. Butler, Bryne T. Ngwenya, Linda A. Kirstein, Frank McDermott, Tiina O'Neill

PII: S0009-2541(22)00559-9

DOI: https://doi.org/10.1016/j.chemgeo.2022.121265

Reference: CHEMGE 121265

To appear in: *Chemical Geology*

Received date: 31 August 2022

Revised date: 7 December 2022

Accepted date: 9 December 2022

Please cite this article as: D.L. Price, I.B. Butler, B.T. Ngwenya, et al., Crystallisation pathways of a mixed La-Nd carbonate – Ambient temperature synthesis of the mineral lanthanite, *Chemical Geology* (2022), https://doi.org/10.1016/j.chemgeo.2022.121265

Title: Crystallisation pathways of a mixed La-Nd carbonate – Ambient temperature synthesis of the mineral Lanthanite

Authors: Dylan L. Price[a]*; Ian B. Butler[a], Bryne T. Ngwenya[a], Linda A. Kirstein[a], Frank McDermott[b], Tiina O'Neill[c]

Corresponding Author: Dylan L. Price. dylan.price@ed.ac.uk. The Grant Institute, The King's Buildings, James Hutton Road, Edinburgh, EH9 3FE. ORCID ID: 0000-0003-4046-7003

Author Affiliations:

[a]School of Geosciences, The University of Edinburgh. The Grant Institute, The King's Buildings, James Hutton Road, Edinburgh EH9 3FE, United Kingdom. Dylan.Price@ed.ac.uk ; Ian.Butler@ed.ac.uk ; Bryne.Ngwenya@ed.ac.uk ; Linda.Kirstein@ed.ac.uk

[b]UCD School of Earth Sciences, University College Dublin, Belfield, Dublin 4, Republic of Ireland. frank.mcdermott@ucd.ie

[c]UCD Conway Imaging Core Facility, Conway Institute, University College Dublin, Belfield, Dublin 4, Republic of Ireland. tiina.oneill@ucd.ie

Abstract:

Naturally occurring rare earth element (REE) bearing carbonate minerals contain different REEs, yet efforts to synthesise and understand their formation mechanisms have hitherto used single REE end-member experiments. In synthesising a mixed La-Nd carbonate, we document how the presence of two REEs affects the overall crystallisation process. We find that the mixed REE carbonate has a broadly similar crystallisation pathway as its end-members but with key differences. The process begins with the precipitation of amorphous spherical nanoparticles which mature into macrocrystals via an intermediary polymorphous phase. The resulting phase is identified as lanthanite, a naturally occurring REE carbonate mineral. The mixed carbonate has unit cell parameters and phase transition times in between that of its La and Nd end-members. Unlike the end-members, the crystallisation

process of mixed REE carbonates has a consistent two-stage transition process between the nanoparticulate and the final phase. They also have a distinct and homogeneous morphology compared to their end-members. These results highlight the importance of considering multiple REEs simultaneously when studying the precipitation mechanisms of REE carbonates.

Keywords:

Rare Earth Carbonate; Aqueous Geochemistry; Time resolved; mixed REE; Precipitation; Lanthanite

1. Introduction

Rare earth elements (REEs) or lanthanoids as per the International Union of Pure and Applied Chemistry (IUPAC) nomenclature are a series of 15 f-block elements from La to Lu (IUPAC, 2005). They are integral to many technological innovations used in the green energy transition (Bobba et al. 2020) as well as in consumer and military goods (Krishnamurthy and Gupta, 2016; Van Gosen et al. 2017; Wilburn, 2012). As a result, demand for these elements has been rising, and is expected to continue to rise in the near to mid future (Roskill, 2021). The REE-bearing minerals of economic interest are principally REE fluorcarbonates (e.g. bastnäsite) and phosphates (e.g. monazite, xenotime), the fluorcarbonates being of slightly greater commercial interest (Zheng and Greedan, 2003).

Despite their name, REEs are not rare in terms of Earth's crustal abundances but rather rarely occur in large, easily exploitable, economic concentrations (Krishnamurthy and Gupta, 2016; Rudnick and Gao, 2003; Weng et al. 2015). Many of the world's large (>1.7 x 10^6 REE tonnes) REE deposits are associated with carbonatite rocks with mineralisation from weathering or hydrothermal alteration and precipitation of REE carbonates and fluorcarbonates (Broom-Fendley et al. 2017; Ling et al. 2013; Ngwenya, 1994; Smith et al. 2016; Walters et al., 2011). REE carbonate minerals are often found as an accessory phase in such deposits (Bhushan and Kumar, 2013; Thi et al., 2014; Zhongxin et al., 1992).

The induced precipitation of REE carbonates is a step sometimes used in ore beneficiation processes to refine REEs (Krishnamurthy and Gupta, 2016; Castor and Hendrick, 2006; Wang et al. 2017).

Additionally, the selective precipitation of REE carbonates is an effective way to extract REEs from toxic acid mine drainage waters (Hassas et al., 2021). Amorphous REE carbonate nanoparticles are useful for their magnetic (Coey et al. 1975) and optical properties (Zhou et al. 2020) and have been used to synthesize ceramic electrolytes for solid oxide fuel cells (Accardo et al. 2019). Some REE carbonates are used as chemical homologues for actinides in the nuclear industry (Kim et al. 2018; Runde et al. 1992). A better understanding of the precipitation pathway of REE carbonates has advantages for the field of geology and material science as well as implications for more efficient REE processing and environmental remediation.

Single-REE carbonates have been synthesised using a range of methods (Jansen et al. 1959; Nagashima et al. 1973; Liu et al. 1999; Refat, 2004). In more recent studies, the crystallisation and precipitation process of these minerals is being investigated with increasing assiduity (Han 2020; Koryttseva and Navrotsky, 2020; Szucs et al. 2021; Vallina et al. 2014; Yu et al. 2020) as REE bearing carbonates are becoming more relevant to technologically advanced goods. However, an often-overlooked parameter is the effect of the presence of multiple REEs in the starting solution on the crystallisation process of REE carbonates. Studies on precipitating REE carbonates from leached low-grade REE ores (Leng et al. 2020; Liu and Ma 1998; Zhang et al. 1995) happen to incorporate multiple REEs into their starting solutions, due to their natural provenance. These works primarily focus on the precipitation and subsequent REE concentration for commercial purposes; therefore, the REEs used in the experiments and their impact on the crystallisation process remained undiscussed. Goncharov et al. (2022) investigated the thermodynamic properties of a mixed La-Nd carbonate synthesised at high temperatures, with the focus being on the end product.

We study the low temperature crystallisation pathways of a mixed La-Nd carbonate at 50:50 and compare the process to that of its single REE carbonate end-members. We use a synthesis method and overall approach similar to the REE carbonate experiments conducted by Rodriguez-Blanco et al. (2014) and Vallina et al. (2015) as their work provides a useful basis for comparison to single REE carbonates.

We find that the mixed REE carbonate has a similar crystallisation pathway to that of its end-member REE counterparts. There are however specific characteristics and behaviours only exhibited in the mixed La-Nd experiments, such as the presence and timings of a two-stage REE uptake into the solid phase as well as a distinct final morphology. The resulting crystals of the mixed La-Nd experiments are mixed La-Nd lanthanite crystals which are structurally and compositionally similar to the naturally occurring lanthanite-Nd mineral $(Nd, La)_2(CO_3)_3 \cdot 8H_2O$.

2. Materials and methods

2.1 Synthesis of REE carbonates

Lanthanum and neodymium carbonates, as well as a mixed La-Nd carbonate, were synthesised following the approach of Rodriguez-Blanco et al. (2014) and Vallina et al. (2015). The La and Nd end-member carbonates were synthesised by adding in equal volumes a 0.01M Na_2CO_3 solution to a 0.01M $REE(NO_3)_3$ solution at 30°C ± 2° with constant stirring. The mixed La-Nd experiment was synthesised by including the respective La and Nd nitrates in equal volumes and combining this with 0.01M Na_2CO_3 whilst maintaining the same $REE:CO_3$ ratio of 1:1 as in the end-member REE experiments. This resulted in a $REE(NO_3)_3$ starting solution comprising of 0.01M $La(NO_3)_3$ and 0.01M $Nd(NO_3)_3$ at a 50:50 La:Nd ratio. The pH was recorded for the starting solutions and immediately upon their mixture. The REE nitrate solutions had a pH of 3.5, 3.8, 3.9 ± 0.2 for the La, Nd and mixed solution respectively. The sodium carbonate solution had a pH of 9.9 ± 0.2. Upon mixing of the starting solutions, the pH of the mixed experiment was measured at 5.8 ± 0.2.

2.2 Real-time and standalone analyses

Following mixing of the starting solutions, and under constant stirring, time resolved absorbance measurements of the solution were recorded to monitor the evolution of the solution. A Camspec M501 UV-Vis spectrophotometer was used to record the absorbance values at 450 nm every 10 seconds and each synthesis was replicated a minimum of 7 times. Through a custom exterior panel to the UV-Vis, an entry and exit tube was connected to the cell holder allowing the circulation of liquid around the cell. An external impeller pump (Huber Ministat 125) circulated heated water to maintain a reaction temperature of 30°C ± 2°. The starting solutions were also pre-heated separately to 30°C ± 2°

prior to mixing. A total of 3.5mL of pre-heated reactant was pipetted into a 1cm cuvette pre-placed inside the machine. The Na_2CO_3 solution was always added to the REE solution. The cell was then covered with a piece of Parafilm "M" and capped with a plastic push-down cap do mitigate evaporation loss. The sample was continually stirred throughout the measurement by a magnetic stirrer inside the UV-Vis. Stirring speed had little to no impact on the sample evolution but it was important that the sample was stirred (A.1).

To generate more material for further analysis, larger volumes (up to 40 mL) of starting solution were used and the samples were prepared outside of the UV-Vis spectrophotometer using the same method. Aliquots of the solution were extracted at set times throughout the growth process, with a minimum of one duplicate for all mixtures. Following Rodriguez-Blanco et al. (2008), the solution was filtered through a 0.2 µm membrane filter; the filter was then washed with ethanol to remove excess water and left to air dry. The filtration and washing were completed in under a minute.

The synthetic REE carbonate was analysed by Scanning Electron Microscopy (SEM), X-Ray Diffraction (XRD) and Transmission Electron Microscopy (TEM) coupled with Selected Area Electron Diffraction (SAED). A Zeiss GeminiSEM A HD VP Field Emission SEM was used to image the material. The sample was coated with a thin 30-60 second gold coat and imaged at 7-10keV. A lower keV was used as the sample was susceptible to charging. A Bruker D2 Phaser diffractometer (wavelength = 1.540 Å; 2Θ = 5-60°) was used to obtain XRD data and the software GSAS II was used to determine unit cell parameters. TEM imaging and selected area electron diffraction (SAED) patterns were obtained from a Tecnai G2 20 Twin TEM at 200keV, where samples were loaded onto 300 mesh carbon formvar coated TEM grids from an ethanol suspension using a microliter pipette. In order to obtain images with minimal exposure to the electron beam, the image was focused in one place and quickly moved to another to obtain a fresh image. The software ImageJ was used to measure the dimensions from the SEM and TEM imaging of the material.

REE partitioning in the precipitated material was determined by isolating the solid phase at set times using centrifuge filters. The solution was prepared as outlined above, but instead of filtering the aliquots with membrane filters, up to 2.5mL of solution was placed in a 3000MWCO centrifugal

filtration tube. The tube was then placed in a centrifuge equipped with a 45 degree fixed angle rotor. The sample was centrifuged at 5500 rpm for 10 minutes where the filtered sample was removed as the supernatant. 10% nitric acid was added to the top half and the tube was once again placed in the centrifuge for 5 minutes. The material collected from this spin was the solid material in the filter now dissolved by the acid and was analysed with a Varian Vista-PRO ICP-OES.

3. Results

3.1 Real-time sample turbidity monitoring

A white, cloudy suspension formed immediately upon mixing of the hitherto transparent REE nitrate and Na_2CO_3 starting solutions. This suspension continued to increase in turbidity with time. The entire process was monitored by a UV-Vis spectrophotometer and showed an initial period of low

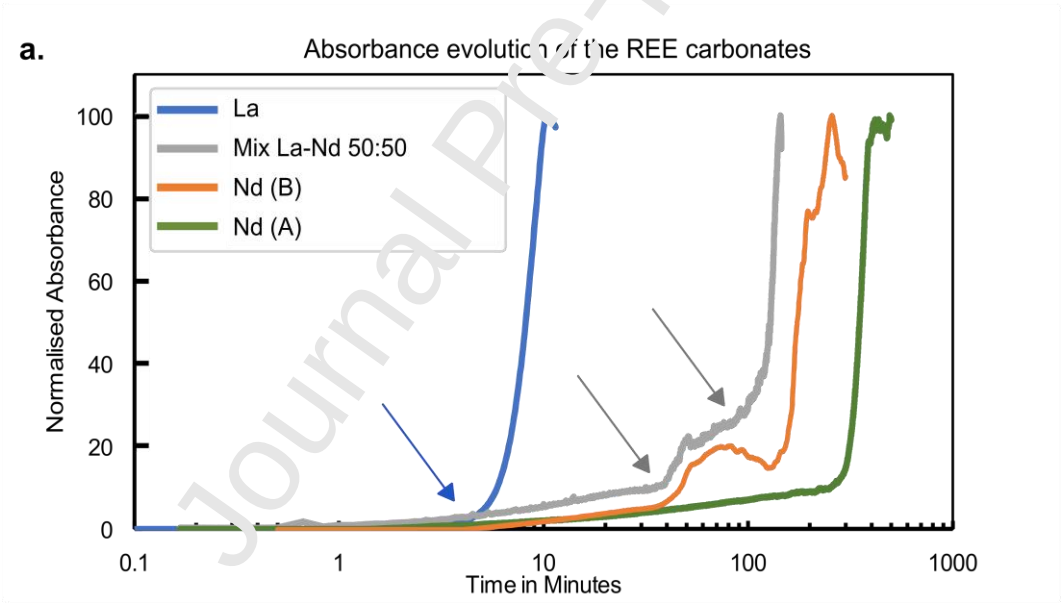

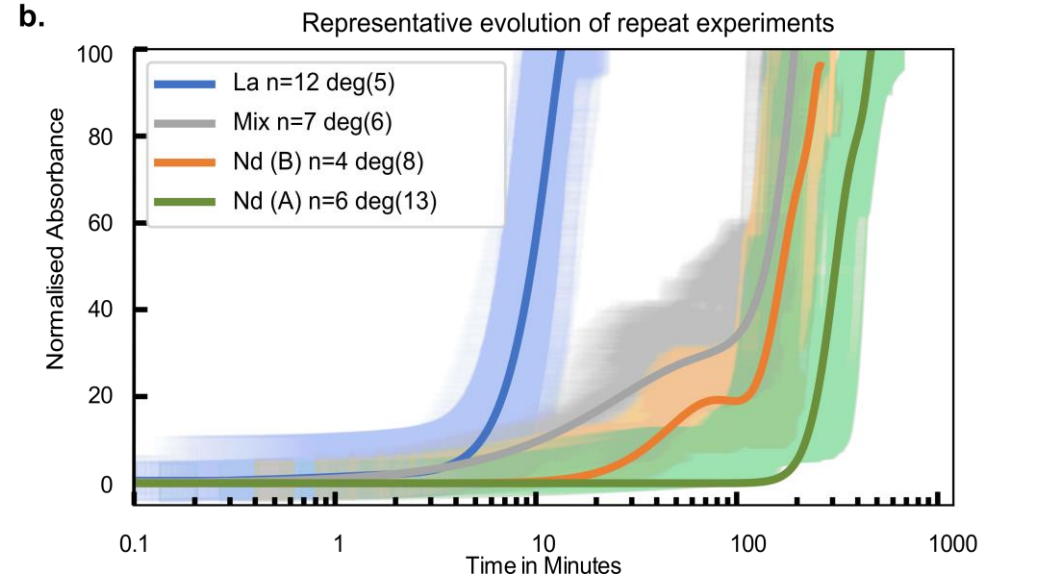

absorbance changing to more rapidly increasing absorbance after a characteristic inflection point (Fig. 1).

Figure 1: (a) Absorbance evolution of REE carbonates. In all cases the origin marks the point of mixing of reactant solutions. For all end-member La experiments and most Nd experiments, after an induction period, the absorbance inflects (e.g. blue arrow) and increases rapidly. The two grey arrows indicate the dual inflection characteristic of all mixed experiments and some Nd experiments. The first inflection is followed by a shoulder or hump in absorbance which is followed by a second, steeper rise in absorbance. The Nd carbonate experiments shown are separated between the single-inflection (Type A) and double-inflection (Type B) absorbance behaviours.

(b) Each measured point is displayed with reduced opacity making areas of overlap from repeat experiments darker to create a "heat map" of common pathways which also shows the variability between repeated experiments. A polynomial fit of all the repeated experiments for La, mixed and Nd carbonates is superimposed on the heat map. n indicates the number of repeat experiments and deg is the degree of the polynomial fit. Individual traces in Fig. A.2

La carbonates showed an increase in absorbance at an inflection time between 4 and 11 minutes, with an average of 5 minutes (n=12; sd= 1) (Fig. 1). The absorbance evolution of Nd carbonates exhibits two distinct behaviours (Type A and Type B, Fig. 1), the occurrence of which does not appear to correlate with any measured experimental parameter. Some experiments show a "double-inflection" (Type B) whilst others have the same absorbance evolution to that of La (Type A). Type A was recorded 6 times compared to 4 times for Type B. Type B sees the absorbance remaining low before a sharp c. 15% increase, marking the first inflection in the double inflection. The first inflection is followed by a period of absorbance stagnation or slight decline before the main second inflection that sees absorbance levels rise rapidly to a maximum. For the Type B Nd experiments, the first inflection occurs between 20-40 (avg. 34, n=4; sd=3) minutes and the main inflection occurs between 100-160 (avg. 122, n=4; sd=18.5) minutes. For Nd experiments with a single inflection absorbance behaviour, inflections occur between 70 to 350 (avg. 151, n=6; sd=67) minutes.

The mixed REE carbonates have a consistent absorbance evolution showing a double-inflection (Fig. 1). The initial inflection times occur between 13 to 40 (avg. 23, n=6; sd=11) minutes and the main one between 95 and 160 (avg. 112, n=6; sd=18) minutes. The variability in the experiments is shown in Fig. 1b.

A representative polynomial fit for each starting solution and a heat map of all the iterations of the experiments (Fig. 1b) shows variability between experiments. The variations within repeat experiments increase for experiments that take longer to reach a maximum absorbance. The heat map

shows the La carbonate behaviour to be more consistent compared to the Nd experiments (Fig. 1). The latter exhibit a range of absorbance evolution behaviours (e.g. single *vs.* double inflections), some of which overlap with the lines of the mixed experiments (Fig. 1).

3.2 Structure and morphology of immediate precipitates

For both the end-member and mixed experiments, the initial cloudy precipitate was analysed by XRD and SAED. This material was collected and filtered within 30 seconds of the mixing of the starting solutions, when the absorbance levels are a stagnant low (Fig. 1).

The precipitates analysed by XRD showed no distinct Bragg peaks, but rather broad humps centred at 18°, 30° and 45°2θ (Fig. 2). Conversely, the SAED pattern showed evidence of a polycrystalline structure (Fig. A.3) and while the TEM images of the material show Moire fringes (Fig. A.3), further experiments found that the crystallisation indicated by the Moire fringes was induced by the TEM beam (Fig. A.4). Repeated scans of the same sample under XRD showed no X-Ray induced crystallisation (Fig. A.5). SEM images show that they also do not grow in size as the sample ages in suspension (Fig. A.6).

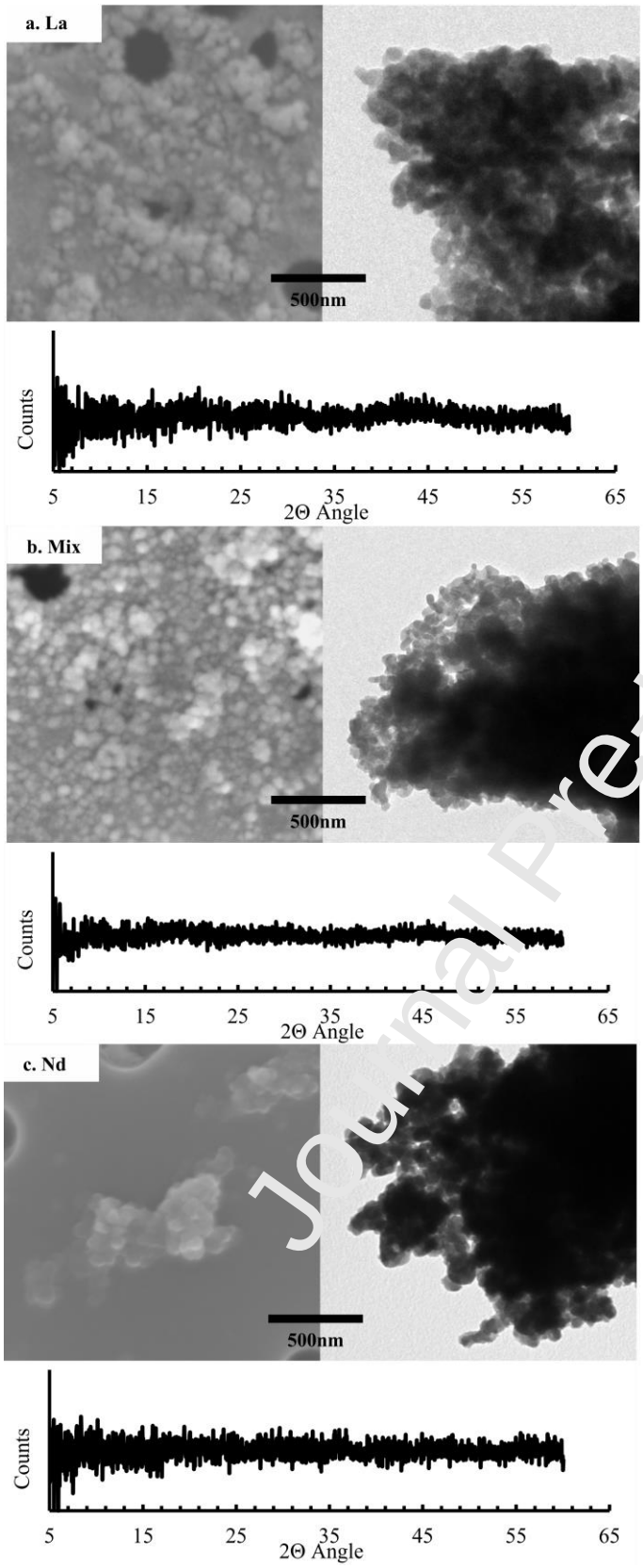

Figure 2: SEM (left) and TEM (right) images for the initial precipitate of La, mixed and Nd carbonate. The images show the morphology and overall disposition of the nanoparticles. Material analysed by SEM were imaged within a 4 days of synthesis and drying whereas the TEM images are of material 7 months after drying. XRD patterns of the initial precipitates for La, the mixed and Nd samples show broad humps.

From TEM and SEM images, these nanoparticles appear broadly spherical and range from 10 to 30 nm in diameter (Fig. 2). Measured from the TEM and SEM images, La particles are on average 24.2 nm (n=140, sd=5.3) in diameter which is slightly larger than the mixed and Nd particles. The mixed experiments average 20.5 nm (n=220, sd=5.5), and Nd are the smallest at 18.3 nm on average (n=156, sd=5.8). Once filtered and dried, these nanoparticles are stable for at least 7 months as they retain their spherical nanoparticulate morphology (Fig. 2).

3.3 Crystal growth and evolution beyond the initial precipitates

For the analysis of mixed precipitates, aliquots of the suspension taken at set times throughout the reaction were analysed to reconcile the relationship between the changing absorbance and the suspended precipitate properties. Due to the variability between repeat experiments, it was not possible to time the sub-sampling of the solution exactly at the inflection point. As such, aliquots were taken before (Fig. 3a), approximately around the inflection (Fig. 3b-d) and after (Fig. 3e-f).

During the initial period of low absorbance, SEM images show the morphologies to be nanoparticles (Fig. 2, Fig. 3a) progressively agglomerating into clusters (Fig. 3b). With time, the surficial areas of the overall nanoparticulate agglomeration began to exhibit a polymorphous character, with sharper, more defined edges (Fig. 3c-e, A.9). This material had multiple shapes and consisted of clusters (up to 1.5 μm) of agglomerated polyhedra and nanoparticles. SEM images in Figure 3c-e illustrate this morphology. XRD analysis of the material show a strong Bragg peak at 10.4 2θ, one at 20.9 2θ and a minor peak at 31.6 2θ. The broad peaks seen for the initial precipitate (Fig. 3 inset) are absent, suggesting the overall sample to be structurally crystalline and no longer primarily comprised of amorphous nanoparticles. The Bragg peaks at 10.4, 20.9 and 31.6 2θ are characteristic of the mineral lanthanite, a naturally occurring REE carbonate octahydrate mineral (ICSD-100027; ICSD-188655) (Fig. A.8).

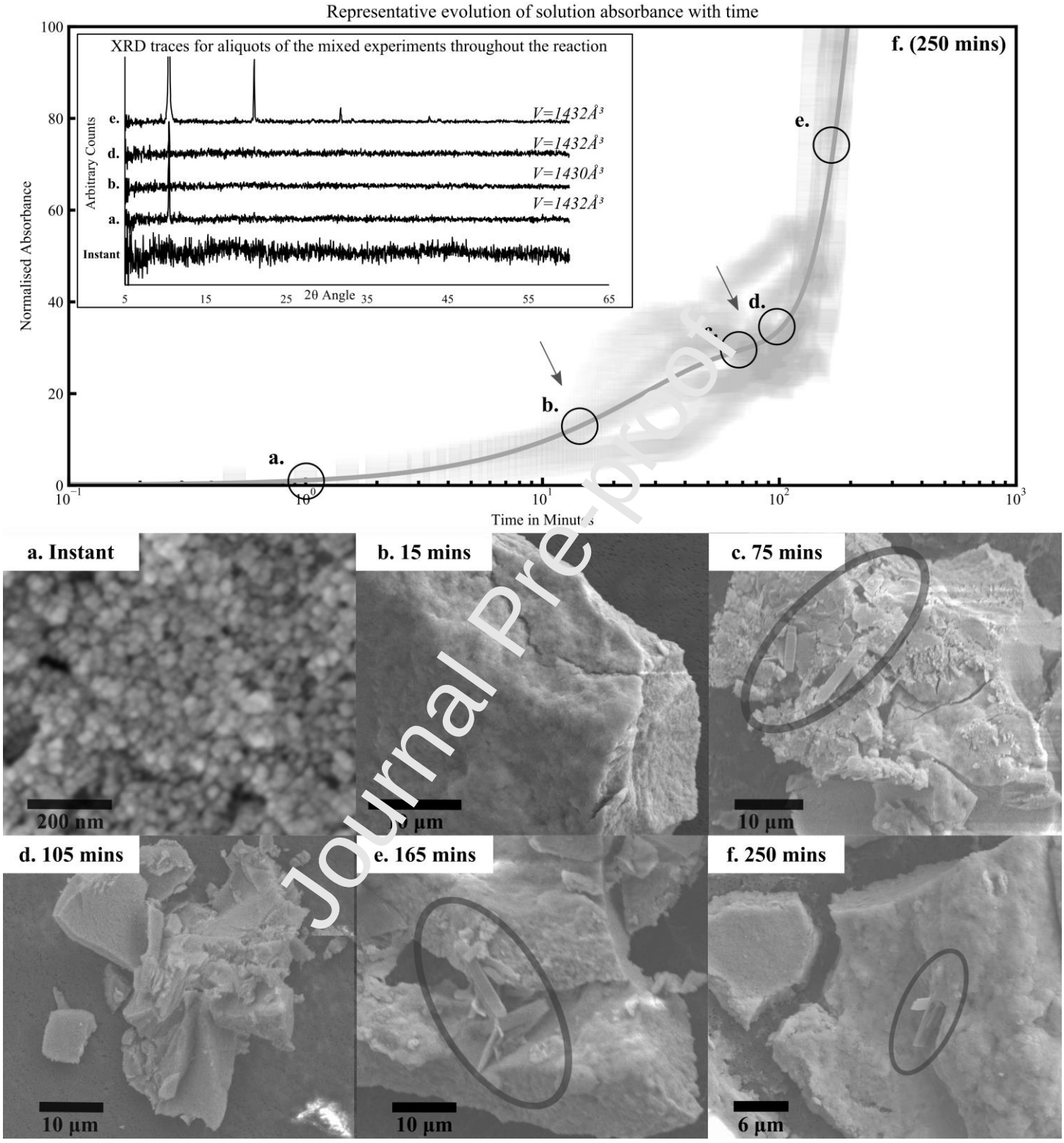

Figure 3: Evolution of the mixed experiment as monitored by UV-Vis, XRD and SEM. The representative absorbance evolution is shown using a polynomial fit and heat-map of all experiment iterations (as in Fig. 1). Circles on the curve correspond to the times at which the SEM images are taken. The inset SEM image labelled instant is taken immediately after the mixing of the starting solutions and shows the initial spherical nanoparticles. Arrows mark the first and main inflections.

Inset: XRD patterns for aliquots taken at various times, with the letters corresponding to their times and V for unit cell volume. Enlarged plot shown in A.7.

At the times surrounding the main inflection in the absorbance levels (Fig. 3c-d), the material observed under SEM is a mixture of the aggregated nanoparticles and polymorphous-appearing material (Fig. A.10). The occasional presence of individual fully-formed crystal laths is encircled on the images (Fig. 3). The material does not appear to change drastically from one aliquot to the next (Fig. 3d-f); the polymorphous material is broadly the same size and the material exhibits a crystalline XRD trace.

At the peak of absorbance and up to 20% of the total time thereafter, the majority of the material still has a polymorphous character with only a limited amount of fully formed single crystals (Fig. 3f). XRD patterns continue to show a distinct lanthanite signature with sharper peaks. The final mixed lanthanite is orthorhombic with a *pccn* space group and unit cell parameters of a= 8.951Å, b= 9.467Å, c= 16.918Å, with a volume of 1430.5Å³. In comparison, the La end-member has unit cell parameters of a= 8.927Å, b= 9.529Å, c= 16.985Å, with a volume of 1444.9Å³ and Nd has a= 8.847Å, b= 9.463Å, c= 17.046Å, with a volume of 1427.2Å³.

The La:Nd ratio of the resulting material for duplicate experiments is shown in Fig. 4. Immediately upon mixing of the starting solutions Nd appears to be preferentially incorporated into the solid phase. The initial solid nanoparticulate phase contains a c. 45:55 La:Nd distribution compared to the

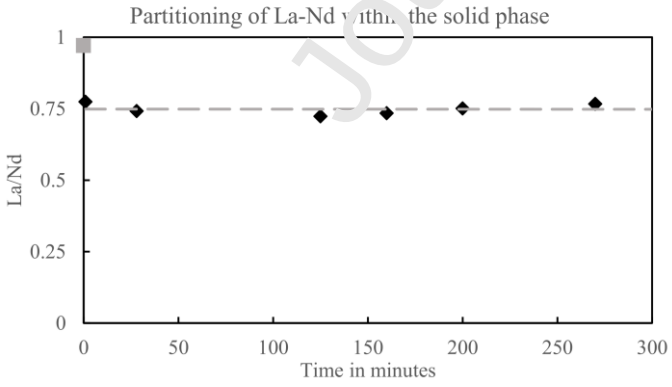

Figure 4: La/Nd ratios within the precipitated material, illustrating the preferential partitioning of Nd into the carbonate phase. The grey marker shows the composition of the starting solution. The synthesis for REE partitioning analysis was conducted twice and the data shown are the average of the two experiments. The error bars for the ICP-OES analytical errors are within the size of the markers and have been omitted.

initial 50:50 and this partitioning bias is maintained at a constant level throughout the growth process (Fig. 4).

3.4 Crystal morphologies

The experimental method produces well-formed and distinct crystals for both REEs and their mixture after significant ageing beyond the UV-Vis absorbance peak. For the mixed REE experiment, the sample is morphologically- and XRD-crystalline in its entirety after 8 hours, without the presence of nanoparticles. Samples aged in aqueous suspension for over 10 days resulted in crystalline products

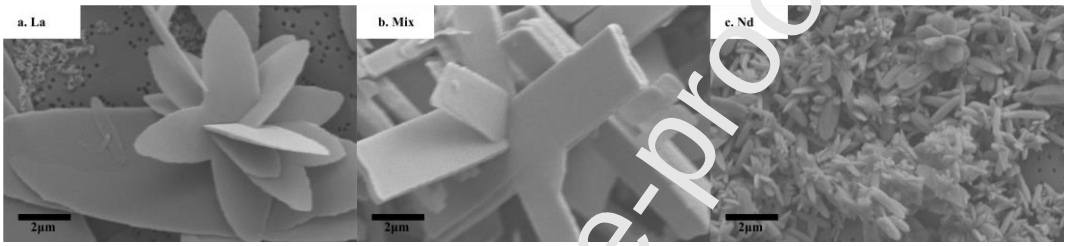

Figure 5: Fully formed crystals of La (a), the mixed La-Nd (b) and Nd (c) carbonate. Stirred until absorbance reaches peak and left in solution for 15, 13 and 17 days respectively.

(Fig. 5).

The crystal habits are specific to the starting solution composition and remain consistent throughout the experiment (Fig. 5). Morphologies vary from units of a distinct habit to rosettes of these units with the same habit. La carbonate crystals appear as symmetrical rosettes (up to 15µm across) comprised of lenticular blades or standalone blades/plates of the same shape (Fig. 5a). The form is time-dependent. Early in the crystallisation process, the blades are individual, with the more mature rosettes only appearing later. The Nd carbonate crystals (up to 3µm) are considerably smaller than those from La carbonates (Fig. 5c). Nd carbonates also appear as rosettes or as discrete crystals. The rosettes differ from the La carbonate examples in that they are made of elongated flat ovoids (Fig. 5c). The mixed experiment exhibits a homogeneous morphology of blades with an orthorhombic form or cruciforms comprised of these blades (up to 10µm in length and 3 µm wide) (Fig. 5b).

4. Discussion

4.1 Absorbance measurements to track crystallisation progress

The UV-vis spectrophotometer provides a real-time measurement of changing absorbance which equates to the proportion of light scattered by the precipitate suspension with time. An increase in light scattering can be due to the presence of larger particles (Amendola and Meneghetti, 2009; Cheng et al. 2010), an increase in particle concentration (Kleizen et al. 1995; Yao et al. 2014), an evolution in particle shape or a change from a monodisperse medium to a polydisperse one due to agglomeration of the particles (Kourti, 2006). A quantitative relationship between the measured absorbance and particle parameters cannot be established for the synthesised experiments, as unlike the aforementioned studies, they do not remain spherical throughout the crystallisation process (Fig. 3). However, results from Melik and Fogler (1982) show that the increase in light scattering can be used as a reliable qualitative indicator for an increase in particle size for a proportion of particles within the suspension. SEM images taken at various points throughout the process give an indication that the inflection may be triggered when much of the XRD-amorphous spherical particles transition to polymorphous agglomerates (Fig. 3, A.11, A.12). In addition to being larger on average, these agglomerates are also more angular, which would result in greater absorbance values for the same material (Begum et al., 2018). Both size and an angular morphology are properties that lead to greater light scattering (Amendola and Meneghetti, 2009; Begum et al., 2018). A change in size leads to an exponential change in absorbance (Kourti, 2006), which explains some local fluctuations in individual experiments (eg. Nd Type P c. 200 minutes or mixed experiment c. 110 minutes in Fig. 1a).

The inflection times of experiments with the same starting solution vary between repeated experiments. Despite the synthesis under controlled and repeatable conditions, there appears to be an intrinsic variability to the crystallisation process. The heatmap in Fig. 1b illustrates this. For experiments with the double inflection, the main inflection has much less variability compared to the first inflection (Fig. 3). This variability increases for experiments with a longer initial nanoparticulate phase. All experiments have this variability, but longer experiments reveal it more markedly (Fig. 1b). Before the period of steep absorbance rise, the sample can contain spherical nanoparticles,

agglomerations thereof, polymorphous material, as well as well-formed crystal blades (Fig. 3, A.10). These morphologies all affect the light scattering in different ways and lead to a timing heterogeneity in development throughout the sample. As such, the longer the initial phase, the greater the variability introduced to the inflection times and propagated throughout the rest of the crystallisation process.

Previous work on single REE carbonates showed a similar light scattering behaviour with the presence of an inflection point proposed to mark the onset of crystallisation with the peak of the absorbance measurements marking the end of the crystallisation reaction (Rodriguez-Blanco et al. 2014; Vallina et al. 2015). Their XRD measurements of the sample at the start of the initial nanoparticulate phase show an XRD amorphous material compared to a lanthanite structure for material taken at the peak of the absorbance measurements (Rodriguez-Blanco et al. 2014; Vallina et al. 2015). Our XRD and SEM analyses of aliquots taken before the inflection and after the peak (Fig. 3) show crystalline material present before the inflection and nanoparticulate material with sparse crystals at, and slightly after, the peak inflection, suggesting that the inflection point is not simply controlled by the onset of crystallisation. Similarly, the maximum absorbance does not correspond to the end of the crystallisation reaction. With newer data acquired at a higher temporal resolution, we suggest a more refined interpretation whereby the absorbance and its inflection are used as a qualitative indicator for the time when a pivoting number of particles become larger and sufficiently crystalline to change the scattering properties of the suspension.

4.2 Effects of mixed REEs in the starting solution

4.2.1 Comparison of mixture with end-members

The timing of the transition from the initial amorphous precursor to the polymorphous aggregates, i.e. the inflection time, is specific to the La:Nd ratio in the starting solution (Figure 1). As such, it must be an innate property of the REEs and their relative amounts that governs the crystallisation process. Previous work by Rodriguez-Blanco et al., (2014) and Vallina et al., (2015) demonstrated that for single end-member REE carbonate syntheses the inflection times for each REE carbonate are correlated to the ionic potential of that REE. The ionic potential is the ratio of the ionic charge (trivalent in this instance) to its ionic radius; a 10-fold coordinated radius is used here for REE in

lanthanite (dal Negro et al., 1977; Morrison et al. 2013). Rodriguez-Blanco et al. (2014) associate the inflection in the absorbance with the end of the dehydration of the hydrated amorphous precursor and the subsequent onset of crystallisation. The REEs with larger ionic potentials, e.g. REEs with lower ionic radii, necessitate a greater energy to dehydrate the amorphous nanoparticulate precursor and thus have later inflection times, with an increasing linear relationship between inflection times and ionic potential for La, Ce, Pr and Nd carbonates (Rodriguez-Blanco et al., 2014).

For a more direct comparison with the published single REE experiments, we can consider our experiments as a La carbonate synthesis heavily doped with Nd, or vice versa. To do this, the averaged ionic potential of the starting solution is used for the mixed experiment. In relation to its end-members, the mixed experiment has an averaged inflection time proportionally related to its mean ionic potential (Fig. 6), suggesting the material to be of homogeneous La-Nd composition. For REE doped calcite, Terakado and Masuda (1988) also noted that REEs interact mutually during the crystallisation process and do not behave as separate units. In our experiments, the overall combination of REEs in the starting solution leads to a corresponding crystallisation behaviour and

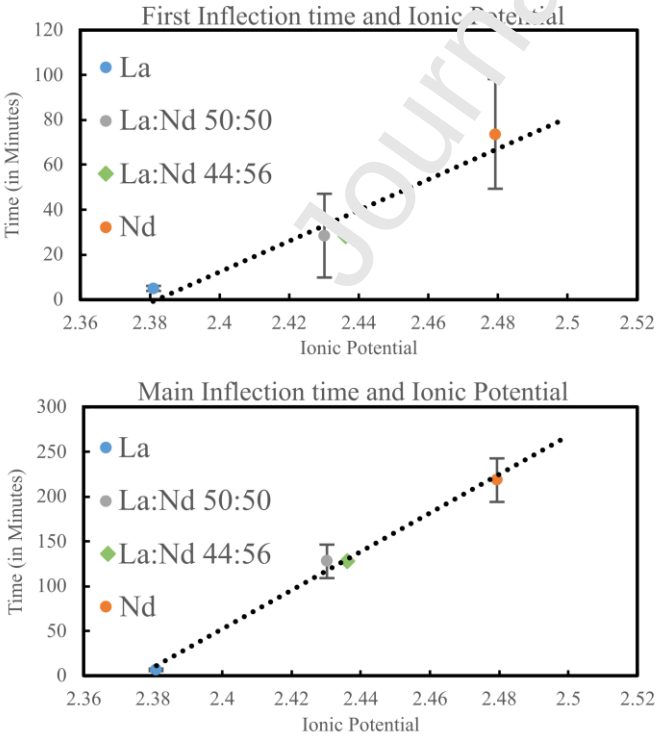

Figure 6: Relationship between averaged inflection time and ionic potential. For experiments with two inflections, the upper graph utilises the first inflection and the lower one the second, main inflection. For experiments with only one inflection, that inflection is in both graphs. The mean ionic potential of the first precipitate of the mixed experiment is also plotted (green diamond); it is within error of the inflection times of the mean ionic potential of the starting solution. Note that a linear relationship stands regardless of which inflection is used, despite the additional difference in inflection times (on the y axis). The ionic radii for the ionic potential calculations are from Jia (1991). The error bars are one standard deviation of the averaged times.

inflection time. The relationship between ionic potential and inflection time noted by Rodriguez-Blanco et al. (2014) applies to the mixed REE carbonates in this study too (Fig. 6).

The main inflection time (Fig. 1) for the mixed experiment is c. 55% between that of the averaged La and Nd times despite the 50:50 starting solution. The inflection times appear to be related to the mean ionic potential of the La:Nd ratio of the first precipitate (45:55) rather than that of the starting solution, although the starting solution REE distribution dictates the REE content of the first precipitates.

Fully formed mixed crystals have a bladed morphology resembling neither of the end-members (Fig. 5). These crystals have a similar morphology and size to Ce carbonates, seen in published work and replicated in supplementary experiments (Fig A.13; Rodriguez-Blanco et al. 2014). The mixed experiment has a similar average ionic potential to that of Ce (2.43 for the mixture *vs.* 2.42 for Ce; compared to 2.38 and 2.48 for La and Nd respectively). As such, there is a possibility that the mean ionic potential of the starting solution would not only impact the crystallisation kinetics but could also influence the morphology of the final crystals.

4.2.2 The double-inflections of the mixed experiments

The inflections in the absorbance evolution of the sample reflect a common mechanism in the crystallisation process and their timings are tied directly to the REE composition of the starting solution. The absorbance evolution of the La-Nd mixture is distinct compared to that of its La and Nd end-members as it consistently possesses two inflections (Fig. 1). The inflections do not translate into straightforward morphological changes, but reflect when the particles reach a critical size and morphology that leads to the increase of their light scattering. For the mixed experiment, SEM images show a slight increase in aggregation of material but a broadly similar morphology of aggregated nanoparticles compared to before and after the inflection (Fig. 3). Some macro-crystalline faces co-exist with distinct nanoparticles and nanoparticle agglomerations (Fig 2, A.10). At the time of the main inflection, the material is polymorphous, having gradually transitioned to this morphology after the first inflection. The partitioning data shows a constant La:Nd ratio over time, suggesting no composition-related controls over the morphology of the particles and therefore light scattering. There

is a possibility that the nanoparticulate phase is comprised of two compositionally distinct phases that would evolve differently. Radha et al. (2012) suggest this for Ca-Mg carbonates. Due to the intimate intermixing of the various particles (Fig. 3), it proved difficult to separate and isolate any material for individual analysis. The XRD data of the crystalline mixed REE material shows a single lanthanite phase present. This also reduces the possibility of a structurally distinct meta-stable intermediary phase, akin to vaterite in calcite precipitation (Christy, 2017; Ogino et al. 1987).

In reference to Ca carbonate analogues (Bots et al. 2012), we can possibly attribute the reduction in absorbance between the two inflections to the dissolution of the nanoparticulate agglomerates as they re-dissolve during Ostwald ripening, thereby reducing the amount and size of particles suspended in solution. Indeed for Ca carbonate systems, published solubility data show the nanoparticles are more soluble than the ensuing, more ordered, vaterite phase at 25°C with Ksp = $10^{-6.3}$ and $10^{-7.9}$ respectively (Brečević and Nielsen, 1989; Plummer and Busenberg, 1982). A minimal reduction of total particle concentration and/or size would lead to a noticeable reduction in the absorbance measurements due to the nature of the UV-Vis' data acquisition process (Kourti, 2006).

It remains unclear as to why the double inflection is consistent in the mixed experiment but only occasional for the Nd end-member. However, the addition of La to the Nd system must be an essential factor to result in such a consistent behaviour.

4.3 Overall crystallisation process

The aqueous, near-ambient temperature, synthesis of a La-Nd mixed carbonate results in the formation of lanthanite with similar composition and structure to natural lanthanite-Nd. We note a general process of crystallisation starting with a spherical amorphous nanoparticulate precursor (c. 15-30nm diameter). These do not grow in size but agglomerate and transition to a meta-stable polymorphous phase before finally resulting in well-formed macro-crystals of up to 15µm via dissolution-reprecipitation. A crystallisation process with similar stages has been noted for single REE carbonates (Kim et al. 2011; Koryttseva and Navrotsky, 2020; Rodriguez-Blanco et al. 2014; Vallina et al. 2013), Ca carbonates (Bots et al. 2012; Blue et al. 2017; Giuffre et al. 2014; Koga et al., 1998; Liu et al., 2008; Neubauer et al., 2022; Ogino et al., 1987; Radha et al. 2010; Schmidt et al. 2014), Ca-

Mg carbonates (Politi et al., 2009; Rodriguez-Blanco et al. 2012), Mg carbonates (Zhang et al. 2007) and Ca-Mg-Fe carbonates (Romanek et al., 2009).

The overall crystallisation process is the same for both end-member and mixed REE carbonates and is summarised in Figure 7. The differences lie in the relative timings of the steps and the morphological differences in the fully-grown crystals. The mixed carbonate's diameter of the spherical nanoparticles, inflection times and unit cell volumes are all in between those of the end-members. The lack of published thermodynamic data for mixed REE carbonates and the amorphous nanoparticles precludes any modelling of the crystallisation process.

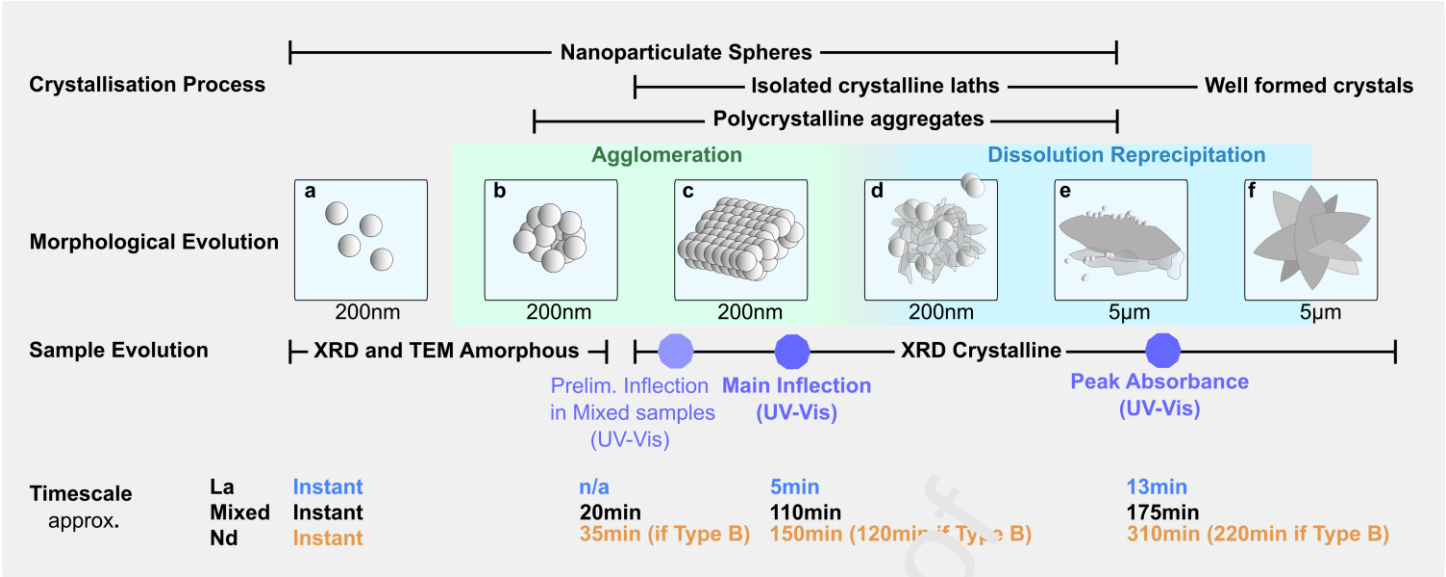

Figure 7: Overall evolution of the crystallisation of mixed and end-member REE carbonates. Note the concurrent presence of many morphologies and their relationship with crystal structure and light scattering.

(a) The first precipitates form almost immediately upon mixing of the starting solutions. Under SEM, they are distinct nanoparticles, which suggests that the agglomeration observed subsequently is not an artefact of the filtering process.
(b) They rapidly agglomerate and form small clusters. This material is XRD and TEM amorphous.
(c) These clusters grow bigger (up to 10µm) and the particles are more compacted together, creating the appearance of a paste comprised of hundreds of nanoparticles. The material is determined from XRD analysis to have the structure of the mineral lanthanite. The absorbance levels have yet to reach their inflection point.
(d) With time, the larger agglomerations begin to exhibit a polymorphous character, with a mixture of spherical nanoparticles and polyhedra. This is the point where most of the amorphous precursor has transformed into the next phase. The occasional crystal blade or lens can be observed among the polymorphous material or isolated on its own.
(e) The polymorphous material transitions from anhedral to more euhedral forms, and thus scattering and absorbing more light, explaining the increase in absorbance after the inflection. A detailed look at the blades reveals ragged edges with the presence of amorphous nanoparticles. This suggests that the crystal blades are formed through a dissolution-precipitation process with the polymorphous material being a nucleation point.
(f) The ratio of polycrystalline material and nanoparticles to crystals decreases with time until the sample is comprised exclusively of crystals. These crystals are morphologically homogeneous and are comprised of individual blades or rosettes thereof. This transition occurs c. 30% of the time after the absorbance levels reach their maximum point.

4.4 Relevance to natural REE carbonate understanding

The synthesized mineral, lanthanite, is a naturally occurring REE carbonate mineral with the general formula of $(REE)_2(CO_3)_3 \cdot 8H_2O$), REE = La, Ce, Nd (Anthony et al., 2003). Lanthanite is commonly found in carbonatite hosted REE deposits as an accessory phase with apatite and REE fluorcarbonate minerals such as synchisite and parisite (Bhushan and Kumar, 2013; Thi et al., 2014; Zhongxin et al., 1992). In such deposits, hydrothermally deposited bastnäsite is the REE mineral of economic interest. Consequently, the formation and/or depositional mechanisms of lanthanite are not well known.

There are also occurrences of major phase lanthanite minerals hosted in carbonate rich rocks that are not associated with larger REE deposits (Cesbron et al. 1979; Coimbra et al., 1989; Coutinho, 1955). These minerals are secondary and are often found superficially or filling fractures, never as massive

units, and can be associated with calcite and malachite. The naturally formed lanthanite tends to be larger than the samples synthesised (up to 1mm) with a platy or tabular habit and sometimes as a rosette, akin to the synthesised experiments (Coutinho, 1955).

Lanthanite is hypothesized to be precipitated from meteoric waters enriched in REE leached from neighbouring minerals (Bevins et al. 1985; Cesbron et al. 1979; Coutinho, 1955; Graham et al. 2007; Weber, 1992) and carbonates tend to be the precipitant of REEs in such waters (Kim et al. 2018). Although there are no exact temperature indicators for the meteoric waters, the temperatures must be below 60°C (Vallina et al. 2015; Williams-Jones and Wood, 1992). Experimental work by Vallina et al. (2015) showed lanthanite-Nd would not form at 60°C, and lanthanite-(La) was only meta-stable at 60°C. The REE content in the waters leading to the precipitation of natural lanthanite is unknown and to not assume water compositions, we used a 50:50 La:Nd ratio of our experiments. Similarly, nitrate was used as a ligand as it is non-complexing, which allows us to isolate the behaviour we observed to the REE. Natural systems may contain sulphate or phosphate ligands which may compete for the REE (Johannesson et al. 1995) and consequently alter the crystallisation kinetics. The measured solution pH of 5.8 following the mixture of the starting solutions would suggest an environment dominated by H_2CO_3 with subordinate HCO_3^- (Stumm and Morgan, 1995).

Lanthanite can contain most REEs in minor quantities. Indeed, some Lanthanite-Ce have equal amounts of structural La and Nd (just as the mixed experiment) at roughly half the amount as Ce and Lanthanite-Nd can have approximately two thirds as much La as Nd (Table 1). It is therefore vital to capture this diversity of REE in the synthesis of lanthanite; our mixed REE experiments illustrate that there is a distinct difference in precipitation behaviour when there are multiple REEs present compared to a single REE.

The resulting synthesised lanthanite has La:Nd ratios and unit cell parameters within range of end-member natural lanthanites (Tables 1 and 2). Some natural lanthanites have more Nd in relation to La (Table 1), pointing to a precipitating fluid containing potentially a greater amount of Nd compared to La, which would be in-line with abundances of REE typically found in groundwater (Noack et al. 2014).

Compared to the end-members, the synthesised mixed lanthanite has both unit cell and compositional similarities with natural Lanthanite-Nd. As such, the mixed experiment is a close analogue to natural samples, especially when compared to synthesised single REE carbonates. As in our experiments, Hassas et al. (2021) used Na_2CO_3 to precipitate REE as carbonates (La as $La_2(CO_3)_3{\cdot}8H_2O$; ie. Lanthanite) and find the carbonate to be a more effective precipitant for acid mine drainage remediation purposes compared with Na_2HPO_4, Na_2SO_4 or $(NH_4)OH$. Information on quantifying the amounts of a certain REE that can be doped into the structure will be advantageous for selective precipitation of REEs, both for environment remediation and ore beneficiation applications. Understanding the influence of REE mixtures on REE carbonate precipitation will also yield a better understanding of mineralisation processes in nature.

Table 1. Comparison of La, Ce and Nd content between this study and natural, non-accessory, lanthanite minerals.

Locality Author(s)	Kirigo, Japan *Nagashima et al. (1986)*	Worldwide *Noak et al. (2014)*	- Present study	Bethlehem, PA, USA *Atencio et al. (1989)*	Curitiba, Brazil *Roberts (1980)*	Whitianga, New Zealand *Graham et al. (2007)*	Bastnäs, Sweden *Atencio et al. (1989)*	North Wales, UK *Bevins et al. (1985)*	Santa Isabel, Brazil *Coimbra et al. (1989)*
Material	Lanthanite-(Nd)	Averaged Groundwater	Mixed sample	Lanthanite-(Nd)	Lanthanite-(Nd)	Lanthanite-(Nd)	Lanthanite-(Ce)	Lanthanite-(Ce)	Lanthanite-(Nd)
La	13.8	22.9	19.8	15.2	16.6	13.5	9.2	12.4	18.0
Ce	1	22.9	-	-	-	8.1	**21.3**	**17.8**	0.2
Nd	**20.5**	**34.6**	**26.6**	**20**	**18.8**	**15.0**	10.1	12.9	**18.6**
La/Nd	0.67	0.66	0.74	0.76	0.88	0.90	0.91	0.96	0.97

Table 1: Comparison of La, Ce and Nd content between this study and natural, non-accessory, lanthanite minerals. Values in bold highlight the most abundant REE. Other REEs and trace elements are not shown. Values shown as REE wt% of lanthanite. Note the lanthanite from this study has a similar La:Nd ratio to Lanthanite-Nd found in the Bethlehem, PA, USA.

Table 2. Unit cell parameters of lanthanite from this study and from natural non-accessory lanthanite

Locality *Author*	Whitianga, New Zealand *Graham et al. (2007)*	- Present study	- Present study	Curitiba, Brazil *Roberts (1980)*	Santa Isabel, Brazil *Coimbra et al. (1989)*	Bastnäs, Sweden *dal Negro et al. (1977)*	North Wales, UK *Bevins et al. (1985)*	- Present study
Material	Lanthanite-(Nd)	Nd Lanthanite	Mixed sample	Lanthanite-(Nd)	Lanthanite-(Nd)	Lanthanite-(Ce)	Lanthanite-(Ce)	La Lanthanite
a	8.923Å	8.847Å	8.931Å	8.942Å	8.941Å	8.937Å	8.965Å	8.927Å
b	9.452Å	9.463Å	9.467Å	9.476Å	9.490Å	9.504Å	9.482Å	9.529Å
c	16.908Å	17.046Å	16.918Å	16.940Å	16.941Å	16.943Å	16.938Å	16.985Å
Volume	1426.0Å³	1427.2Å³	1430.5Å³	1435.4Å³	1437.4Å³	1439.1Å³	1439.8Å³	1444.9Å³
La/Nd	0.90	-	0.78	0.88	0.97	0.91	0.96	-

Table 2: Unit cell parameters of lanthanite from this study and from natural non-accessory lanthanite obtained from the software GSAS II. The unit cell of lanthanite belongs to space group 56, *pccn*. Unit cell parameters show differences in cell volume between Lanthanite-Nd and -Ce and shows the synthesised mixed lanthanite in between the dimensions of La and Nd. The REEs in lanthanite have a 10-fold coordination (dal Negro et al. 1977; Morrison et al. 2013). In such a configuration, the ionic radii of La and Ce are quite similar and smaller than that Nd (La^{3+}=1.27; Ce^{3+}=1.25; Nd^{3+}=1.21. Jia, 1991). It is expected for Lanthanite-Ce's unit cell to be larger than that of Lanthanite-Nd and consequently for La Lanthanite to be the largest. Within the same end-members, there is no trend between unit cell volumes and minor variations in La, Ce and Nd compositions.

5. Conclusions

The presence of multiple REEs in the starting solution has an impact on the subsequent crystallisation process as the mixed experiment consistently exhibited a double-inflection behaviour that the end-members did not have. REE carbonates synthesised from a mixed REE starting solution have a multi-step crystallisation process with two inflections and many intermediate steps before reaching a final morphologically crystalline form. This is opposed to a more straightforward process seen for end-member REEs with the amorphous precursor followed by linear crystal growth. For the mixed REE carbonates, we also see a fractionation of REEs during the growth process which is related to the starting solution. The fully-formed crystals are morphologically homogeneous and distinct from the single REE end-members.

An ideal single-REE bearing solution does not exist in natural geological systems as multiple REEs are always present at various concentrations. We demonstrate that REE diversity in syntheses is a crucially overlooked aspect in previous work. La and Nd are both light REEs with different but broadly similar radii and properties compared to heavy REE; mixtures between REEs with further differences should yield a crystallisation process with even more complications. Additionally, a better understanding of the crystallisation pathways of mixed REE carbonates of various ratios and REEs will lead to a better representation of processes in natural REE forming geological systems.

Acknowledgments and Funding: This work was supported by a NERC Doctoral Training Partnership grant (NE/L002558/1). The authors would like to acknowledge their colleague Laetitia Pichevin for conducting the ICP-OES analyses of the samples. For the purpose of open access, the author has applied a Creative Commons Attribution (CC BY) licence to any Author Accepted Manuscript version arising from this submission.

References

Accardo, G., Dell'Agli, G., Mascolo, M. C., Spiridigliozzi, L., & Yoon, S. P. (2019). Controlled coprecipitation of amorphous cerium-based carbonates with suitable morphology as precursors of ceramic electrolytes for IT-SOFCs. *Materials, 12*(5).

Amendola, V., & Meneghetti, M. (2009). Size evaluation of gold nanoparticles by UV-vis spectroscopy. *Journal of Physical Chemistry C*, *113*(11), 4277–4285.

Anthony, J. W. et al. (2003) Handbook of Mineralogy Crystal Data, Mineralogical Society of America.

Atencio, D., Bevins, R., Fleischer, M., Terry Williams, C., & Williams, P. (1989). Revision of the lanthanite group and new data for specimens from Bastnäs, Sweden, and Bethlehem, USA. Mineralogical Magazine, 53(373), 639-642.

Begum, R., Farooqi, Z. H., Naseem, K., Ali, F., Batool, M., Xiao, J., & Irfan, A. (2018). Applications of UV/Vis spectroscopy in characterization and catalytic activity of noble metal nanoparticles fabricated in responsive polymer microgels: a review. *Critical reviews in analytical chemistry*, *48*(6), 503-516.

Bevins RE, Rowbotham G, Stephens FS, Turgoose S, W. P. (1985). Lanthanite-(Ce),(Ce, La, Nd) 2 (CO3) 3· 8H2O, a new mineral from Wales, UK. *American Mineralogist*, *70*, 411–413.

Bhushan, S. K., & Kumar, A. (2013). First carbonatite hosted REE deposit from India. Journal of the Geological Society of India, 81(1), 41–60.

Blue, C. R., Giuffre, A., Mergelsberg, S., Han, N., De Yoreo, J. J., & Dove, P. M. (2017). Chemical and physical controls on the transformation of amorphous calcium carbonate into crystalline CaCO3polymorphs. *Geochimica et Cosmochimica Acta*, *196*, 179–196.

Bobba, S., Carrara, S., Huisman, J., Mathieux, F., & Pavel, C. (2020). Critical Raw Materials for Strategic Technologies and Sectors in the EU—A Foresight Study. *European Commission: Brussels, Belgium*.

Bots, P., Benning, L. G., Rodriguez-Blanco, J. D., Roncal-Herrero, T., & Shaw, S. (2012). Mechanistic insights into the crystallization of amorphous calcium carbonate (ACC). *Crystal Growth and Design*, *12*(7), 3806–3814.

Brečević, L. and Nielsen, A.E., (1989). Solubility of amorphous calcium carbonate. *Journal of crystal growth*, *98*(3), pp.504-510.

Broom-Fendley, S., Brady, A., Wall, F., Gunn, G., & Dawes, W. (2017). REE minerals at the Songwe Hill carbonatite, Malawi HREE-enrichment in late-stage apatite. *Ore Geology Reviews*, 23–41.

Castor, S. B., & Hendrick, J. B. (2006). Rare Earth Elements. *Industrial Minerals & Rocks: Commodities, Markets, and Uses*, 769–792.

Cesbron, F., Sichère, M.-C., Vachey, H., Cassedanne, J., & Cassedanne, J. O. (1979). La lanthanite à europium du Curitiba, Paraná, Brésil. Bulletin de Minéralogie, 102(4), 342–347. (in French)

Cheng, W. P., Chen, W. Y., Yu, R. F., & Hsieh, Y. J. u. (2010). The Relationship Between Particle Size and Turbidity Fluctuations in Coagulation Process. *Journal of Residuals Science & Technology*, *7*(2), 87–94.

Christy, A.G., 2017. A Review of the Structures of Vaterite: The Impossible, the Possible, and the Likely. Cryst. Growth Des. 17, 3567–3578.

Coey, J. M. D., Chappert, J., Rebouillat, J. P., & Wang, T. S. (1976). Magnetic structure of an amorphous rare-earth transition-metal alloy. *Physical Review Letters*, *36*(17), 1061–1064.

Coimbra, A. M., Coutinho, J. M. V, Antenucio, D., & Iwanuch, W. (1989). Lanthanite-(Nd) from Santa Isabel, State of Sao Paulo: Second Brazilian and world occurence. Canadian Mineralogist, 27, 119–123.

Coutinho, J. M. V. (1955). Lantanita de Curitiba, Paraná. Boletim Da Faculdade de Filosofia, Ciências e Letras Da Universidade de São Paulo. Mineralogia, 13, 119–126. (in Portuguese)

Dal Negro, A., Rossi, G., & Tazzoli, V. (1977). The crystal structure of lanthanite. *American Mineralogist*, *62*((1-2)), 142–146.

Giuffre, A. J., Gagnon, A. C., De Yoreo, J. J., & Dove, P. M. (2015). Isotopic tracer evidence for the amorphous calcium carbonate to calcite transformation by dissolution-reprecipitation. *Geochimica et Cosmochimica Acta*, *165*, 407–417.

Goncharov, V. G., Nisbet, H., Strzelecki, A., Benmore, C. J., Migdisov, A. A., Xu, H., & Guo, X. (2022). Energetics of Hydroxylbastnäsite Solid Solutions, La1-xNd CO3OH. *Geochimica et Cosmochimica Acta, 330*, 47-66

Graham, I., Pogson, R., Colchester, D., Hergt, J., Martin, R., & Williams, P. (2007). Pink lanthanite-(Nd) from Whitianga quarry, Coromandel Peninsula, New Zealand. *The Canadian Mineralogist*, *45*, 1389–1396.

Han, K. N. (2020). Characteristics of precipitation of rare earth elements with various precipitants. *Minerals*, *10*(2).

Hassas, B. V., Rezaee, M., & Pisupati, S. V. (2021). Effect of various ligands on the selective precipitation of critical and rare earth elements from acid mine drainage. *Chemosphere*, *280*(May), 130684.

IUPAC. (2005). Nomenclature of Inorganic Chemistry. IUPAC Recommendations 2005. RSC Publishing

Jansen, G. J., Magin, G. B. J., & Levin, B. (1959). Synthesis of Bastnäsite. *The American Mineralogist*, *44*(October), 1–2.

Jia, Y. Q. (1991). Crystal radii and effective ionic radii of the rare earth ions. *Journal of Solid State Chemistry*, *95*(1), 184–187.

Johannesson, K. H., Lyons, W. B., Stetzenbach, K. J., & Byrne, R. H. (1995). The solubility control of rare earth elements in natural terrestrial waters and the significance of PO43- and CO32- in limiting dissolved rare earth concentrations: A review of recent information. *Aquatic Geochemistry*, *1*(2), 157–173.

Kim, P., Anderko, A., Navrotsky, A., & Riman, R. (2018). Trends in Structure and Thermodynamic Properties of Normal Rare Earth Carbonates and Rare Earth Hydroxycarbonates. *Minerals*, *8*(3), 106.

Kim, J. M., Chang, S. M., Kim, K. S., Chung, M. K., & Kim, W. S. (2011). Acoustic influence on aggregation and agglomeration of crystals in reaction crystallization of cerium carbonate. *Colloids and Surfaces A: Physicochemical and Engineering Aspects*, *375*(1–3), 193–199.

Kleizen, H. H., De Putter, A. B., Van der Beek, M., & Huynink, S. J. (1995). Particle concentration, size and turbidity. *Filtration & separation*, *32*(9), 897-901.

Koga, N. (1998). Crystallization of amorphous calcium carbonate. *Thermochimica Acta*, *318*(1–2), 239–244.

Koryttseva, A., & Navrotsky, A. (2020). Formation and energetics of amorphous rare earth (RE) carbonates in the RE2O3–CO2–H2O system. *Thermochimica Acta*, *692*(August), 178753.

Kourti, T. (2006). Turbidimetry in Particle Size Analysis. *Encyclopedia of Analytical Chemistry*.

Krishnamurthy, N., & Gupta, C. K. (2016). *Extractive Metallurgy of Rare Earths* (Second Edi). CRC Press.

Leng, Z. Y., Liu, S. Z., Ma, Y., Xu, Y. H., Wang, W. B., Hao, X. K., Bai, Y., Fan, M. Y., Huang, J. M., Wu, J. J. (2000). Precipitation of crystalline rare earth carbonate from concentrated sulfuric acid roasting water leaching solution. *Chinese Rare Earths.* 21(2). (in Chinese)

Ling, M. X., Liu, Y. L., Williams, I. S., Teng, F. Z., Yang, X. Y., Ding, X., … Sun, W. D. (2013). Formation of the world's largest REE deposit through protracted fluxing of carbonatite by subduction-derived fluids. *Scientific Reports*, *3*, 1–8.

Liu, J., Rieger, J., & Huber, K. (2008). Analysis of the Nucleation and Growth of Amorphous CaCO3 by Means of Time-Resolved Static Light Scattering. *Society*, (13), 5123–5125.

Liu, S. and Ma, R., (1998). Preparation of crystalline precipitation of mixed rare earth carbonates. *The Chinese Journal of Nonferrous Metals*, *8*(2), pp.331-334. (in Chinese)

Liu, S., Ma, R., Jiang, R., & Luo, F. (1999). Synthesis and structure of hydrated neodymium carbonate. *Journal of Crystal Growth*, *203*(3), 454–457.

Melik, D. H., & Fogler, H. S. (1983). Turbidimetric determination of particle size distributions of colloidal systems. *Journal of Colloid and Interface Science*, *92*(1), 161–180.

Morrison, S.M., Andrade, M.B., Wenz, M.D., Domanik, K.J. and Downs, R.T., 2013. Lanthanite-(Nd), Nd2 (CO3) 3· 8H2O. Acta Crystallographica Section E: Structure Reports Online, 69(3), pp.i15-i16.

Nagashima, K., Wakita, H., & Mochizuki, A. (1973). The synthesis of crytalline rare earth carbonates. *Bulletin of the Chemical Society of Japan*, *46*(1), 152–156.

Nagashima, K. et al. (1986) Kimuraite, CaY2(CO3)4.6H2O, a new mineral from fissures in an alkali olivine basalt from Saga Prefecture, Japan, and new data on lokkaite., American Mineralogist, 71(7–8), pp. 1028–1033.

Neubauer, T. M., Serpa, F. S., Franceschi, E., Dariva, C., Sayer, C., Hermes De Araújo, P. H., Barbosa Castro, B., Aldeia, W., & Da Costa, C. (2022). Crystallization of Calcium Carbonate: Modeling Thermodynamic Equilibrium, Pathway, Nucleation, Growth, Agglomeration, and Dissolution Kinetics with the Presence of Mg2+, Ba2+, and Sr2+. *Industrial and Engineering Chemistry Research*.

Ngwenya, B. T. (1994). Hydrothermal rare earth mineralisation in carbonatites of the Tundulu complex, Malawi: Processes at the fluid/rock interface. *Geochimica et Cosmochimica Acta*, *58*(9), 2061–2072.

Noack, C. W., Dzombak, D. A., & Karamalidis, A. K. (2014). Rare earth element distributions and trends in natural waters with a focus on groundwater. *Environmental Science and Technology*, *48*(8), 4317–4326.

Ogino, T., Suzuki, T., & Sawada, K. (1987). The formation and transformation mechanism of calcium carbonate in water. *Geochimica et Cosmochimica Acta*, *51*(10), 2757–2767.

Plummer, L.N. and Busenberg, E., (1982). The solubilities of calcite, aragonite and vaterite in CO2-H2O solutions between 0 and 90 C, and an evaluation of the aqueous model for the system CaCO3-CO2-H2O. *Geochimica et cosmochimica acta*, *46*(6), pp.1011-1040.

Politi, Y., Batchelor, D. R., Zaslansky, P., Chmelka, B. F., Weaver, J. C., Sagi, I., … Addadi, L. (2010). Role of magnesium ion in the stabilization of biogenic amorphous calcium carbonate: A structure-function investigation. *Chemistry of Materials*, *22*(1), 161–166.

Radha, A. V., Forbes, T. Z., Killian, C. E., Gilbert, P. U. P. A., & Navrotsky, A. (2010). Transformation and crystallization energetics of synthetic and biogenic amorphous calcium carbonate. *Proceedings of the National Academy of Sciences*, *107*(38), 16438–16443.

Radha, A. V., Fernandez-Martinez, A., Hu, Y., Jun, Y.S., Waychunas, G.A., Navrotsky, A., 2012. Energetic and structural studies of amorphous Ca 1-xMg xCO 3·nH 2O (0≤x≤1). Geochim. Cosmochim. Acta 90, 83–95.

Refat, M. S. (2004). A novel method for the synthesis of rare earth carbonates. *Synthesis and Reactivity in Inorganic and Metal-Organic Chemistry*, *34*(9), 1605–1613.

Roberts, A. C., Chao, G. Y., & Cesbron, F. (n.d.). Lanthanite-(Nd), A new mineral from Curitiba, Parana, Brazil. 1980, 1–2.

Rodriguez-Blanco, J. D., Shaw, S., & Benning, L. G. (2008). How to make "stable" ACC: protocol and preliminary structural characterization. *Mineralogical Magazine*, *72*(1), 283–286.

Rodriguez-Blanco, J. D., Shaw, S., Bots, P., Roncal-Herrero, T., & Benning, L. G. (2012). The role of pH and Mg on the stability and crystallization of amorphous calcium carbonate. *Journal of Alloys and Compounds*, *536*(SUPPL.1), A.477–A.479.

Rodriguez-Blanco, J. D., Vallina, B., Blanco, J. A., & Benning, L. G. (2014). The role of REE3+ in the crystallization of lanthanites. *Mineralogical Magazine*, *78*(6), 1373–1380.

Romanek, C. S., Jiménez-López, C., Navarro, A. R., Sánchez-Román, M., Sahai, N., & Coleman, M. (2009). Inorganic synthesis of Fe-Ca-Mg carbonates at low temperature. *Geochimica et Cosmochimica Acta*, *73*(18), 5361–5376.

Roskill (2021). Rare Earths Outlook to 2030, 20th Edition.

Rudnick, R. L. and Gao, S. (2013) *Composition of the Continental Crust*. 2nd edn, *Treatise on Geochemistry: Second Edition*. 2nd edn. Elsevier Ltd.

Runde, W., Meinrath, G. and Kim, J.I., (1992). A study of solid-liquid phase equilibria of trivalent lanthanide and actinide ions in carbonate systems. *Radiochimica Acta*, *58*(1), pp.93-100.

Schmidt, M. P., Ilott, A. J., Phillips, B. L., & Reeder, R. J. (2014). Structural changes upon dehydration of amorphous calcium carbonate. *Crystal Growth and Design*, *14*(3), 938–951.

Smith, M. P., Moore, K., Kavecsánszki, D., Finch, A. A., Kynicky, J., & Wall, F. (2016). From mantle to critical zone: A review of large and giant sized deposits of the rare earth elements. *Geoscience Frontiers*, *7*(3), 315–334.

Stumm, W. and Morgan, J. (1996) *Aquatic chemistry : chemical equilibria and rates in natural waters / Werner Stumm, James J. Morgan.* Third edition. Wiley. New York.

Szucs, A. M., Stavropoulou, A., O'Donnell, C., Davis, S., & Rodriguez-Blanco, J. D. (2021). Reaction Pathways toward the Formation of Bastnäsite: Replacement of Calcite by Rare Earth Carbonates. *Crystal Growth and Design*, *21*(1), 512–527.

Terakado, Y., & Masuda, A. (1988). The coprecipitation of Rare-Earth Elements With Calcite and Aragonite. *Chemical Geology*, *69*, 103–110.

Thi, T. N., Wada, H., Ishikawa, T., & Shimano, T. (2014). Geochemistry and petrogenesis of carbonatites from South Nam Xe, Lai Chau area, northwest Vietnam. *Mineralogy and Petrology*, *108*(3), 371–390.

Vallina, B., Rodriguez-Blanco, J. D., Brown, A. P., Blanco, J. A., & Benning, L. G. (2013). Amorphous dysprosium carbonate: characterization, stability, and crystallization pathways. *Journal of Nanoparticle Research*, *15*(2), 1-13.

Vallina, B., Rodriguez-Blanco, J. D., Blanco, J. A., & Benning, L. G. (2014). The effect of heating on the morphology of crystalline neodymium hydroxycarbonate, NdCO3OH. *Mineralogical Magazine*, *78*(6), 1391–1397.

Vallina, B., Rodriguez-Blanco, J. D., Brown, A. P., Blanco, J. A., & Benning, L. G. (2015). The role of amorphous precursors in the crystallization of La and Nd carbonates. *Nanoscale*, *7*(28), 12166–12179.

Van Gosen, B. S., Verplanck, P. L., Seal II, R. R., Long, K. R., & Gambogi, J. (2017). *Rare-earth elements* (No. 1802-O). US Geological Survey.

Waber, N. (1992). The supergene thorium and rare-earth element deposit at Morro do Ferro, Poços de Caldas, Minas Gerais, Brazil. *Journal of Geochemical Exploration*, *45*(1–3), 113–157.

Walters A., Lusty P., Hill A. (2011) Rare earth elements. *Mineral Profile Series*, British Geological Survey, United Kingdom, 54 pp

Wang, L., Huang, X., Yu, Y., Zhao, L., Wang, C., Feng, Z., … Long, Z. (2017). Towards cleaner production of rare earth elements from bastnaesite in China. *Journal of Cleaner Production*, *165*(2), 231–242.

Weng, Z., Jowitt, S. M., Mudd, G. M., & Haque, N. (2015). A Detailed Assessment of Global Rare Earth Element Resources- Opportunities and Challenges. *Economic Geology*, *110*(October), 1925–1952.

Wilburn, D. R. (2012). *Byproduct Metals and Rare-earth Elements Used in the Production of Light-emitting Diodes: Overview of Principal Sources of Supply and Material Requirements for Selected Markets*. US Department of the Interior, US Geological Survey.

Williams-Jones, A. E., & Wood, S. A. (1992). A preliminary petrogenetic grid for REE fluorocarbonates and associated minerals. *Geochimica et Cosmochimica Acta*, *56*(2), 725–738.

Yao, M., Nan, J., & Chen, T. (2014). Effect of particle size distribution on turbidity under various water quality levels during flocculation processes. *Desalination*, *354*, 116–124.

Yu, Z., Wang, M., Wang, L., Zhao, L., Feng, Z., Sun, X., & Huang, X. (2020). Preparation of crystalline mixed rare earth carbonates by $Mg(HCO_3)_2$ precipitation method. *Journal of Rare Earths*, *38*(3), 292–298.

Zhang, L. Y., Wu, Z. H., Zhang, H. J. (1995). The technological study of preparing mixed rare earth carbonate by way of precipitation with ammonium bicarbonate. *Journal of Baotou University of Iron and Steel Technology*. 14(3). (in Chinese)

Zhang, Z., Zheng, Y., Zhang, J., Zhang, Q., Chen, J., Liu, Z., & Liang, X. (2007). Synthesis and shape evolution of monodisperse basic magnesium carbonate microspheres. *Crystal Growth and Design*, *7*(2), 337–342.

Zheng, Z., & Greedan, J. E. (2003). Rare Earth Elements and Materials. *Encyclopedia of Physical Science and Technology*, *57*, 1–22.

Zhongxin, Y., Ge, B., Chenyu, W., Zhongqin, Z., & Xianjiang, Y. (1992). Geological features and genesis of the Bayan Obo REE ore deposit, Inner Mongolia, China. *Applied Geochemistry*, *7*(5), 429–442.

Zhou, J., Shi, D., & Chen, M. (2020). Bio-inspired mineral fluorescent hydrogels cross-linked by amorphous rare earth carbonates. *Chemical Communications*, *56*(88), 13646–13648.

Declaration of interests

☒The authors declare that they have no known competing financial interests or personal relationships that could have appeared to influence the work reported in this paper.

☐The authors declare the following financial interests/personal relationships which may be considered as potential competing interests:

Table 1. Comparison of La, Ce and Nd content between this study and natural, non-accessory, lanthanite minerals. Other REEs and trace elements are not shown. (REE wt% of lanthanite)

Locality Author(s)	Kirigo, Japan *Nagashima et al. (1986)*	Worldwide *Noak et al. (2014)*	- Present study	Bethlehem, PA, USA *Antencio et al. (1989)*	Curitiba, Brazil *Roberts (1980)*	Whitianga, New Zealand *Graham et al. (2007)*	Bastnäs, Sweden *Atencio et al. (1989)*	North Wales, UK *Bevins et al. (1985)*	Santa Isabel, Brazil *Coimbra et al. (1989)*
Material	Lanthanite-(Nd)	Averaged Groundwater	Mixed sample	Lanthanite-(Nd)	Lanthanite-(Nd)	Lanthanite-(Nd)	Lanthanite-(Ce)	Lanthanite-(Ce)	Lanthanite-(Nd)
La	13.8	22.9	19.8	15.2	16.6	13.5	9.2	12.4	18.0
Ce	1	22.9	-	-	-	8.1	**21.3**	**17.8**	0.2
Nd	**20.5**	**34.6**	**26.6**	**20**	**18.8**	**15.0**	10.1	12.9	**18.6**
La/Nd	0.67	0.66	0.74	0.76	0.88	0.90	0.91	0.96	0.97

Table 2. Unit cell parameters of lanthanite from this study and from natural non-accessory lanthanite

Locality *Author(s)*	Whitianga, New Zealand *Graham et al. (2007)*	- Present study	- Present study	Curitiba, Brazil *Roberts (1980)*	Santa Isabel, Brazil *Coimbra et al. (1989)*	Bastnäs, Sweden *dal Negro et al. (1977)*	North Wales, UK *Bevins et al. (1985)*	- Present study
Material	Lanthanite-(Nd)	Nd Lanthanite	Mixed sample	Lanthanite-(Nd)	Lanthanite-(Nd)	Lanthanite-(Ce)	Lanthanite-(Ce)	La Lanthanite
a	8.923Å	8.847Å	8.951Å	8.942Å	8.941Å	8.937Å	8.965Å	8.927Å
b	9.452Å	9.463Å	9.467Å	9.476Å	9.490Å	9.504Å	9.482Å	9.529Å
c	16.908Å	17.046Å	16.918Å	16.940Å	16.941Å	16.943Å	16.938Å	16.985Å
Volume	1426.0Å³	1427.2Å³	1430.5Å³	1435.4Å³	1437.4Å³	1439.1Å³	1439.8Å³	1444.9Å³
La/Nd	0.90	-	0.78	0.83	0.97	0.91	0.96	-

Highlights

- All naturally occurring REE carbonates contain more than one REE
- We synthesized a mixed La-Nd carbonate and monitored its crystallisation
- It has a different crystallisation pathway compared to single REE carbonates
- The resulting crystals have a homogeneous and mixed REE specific morphology

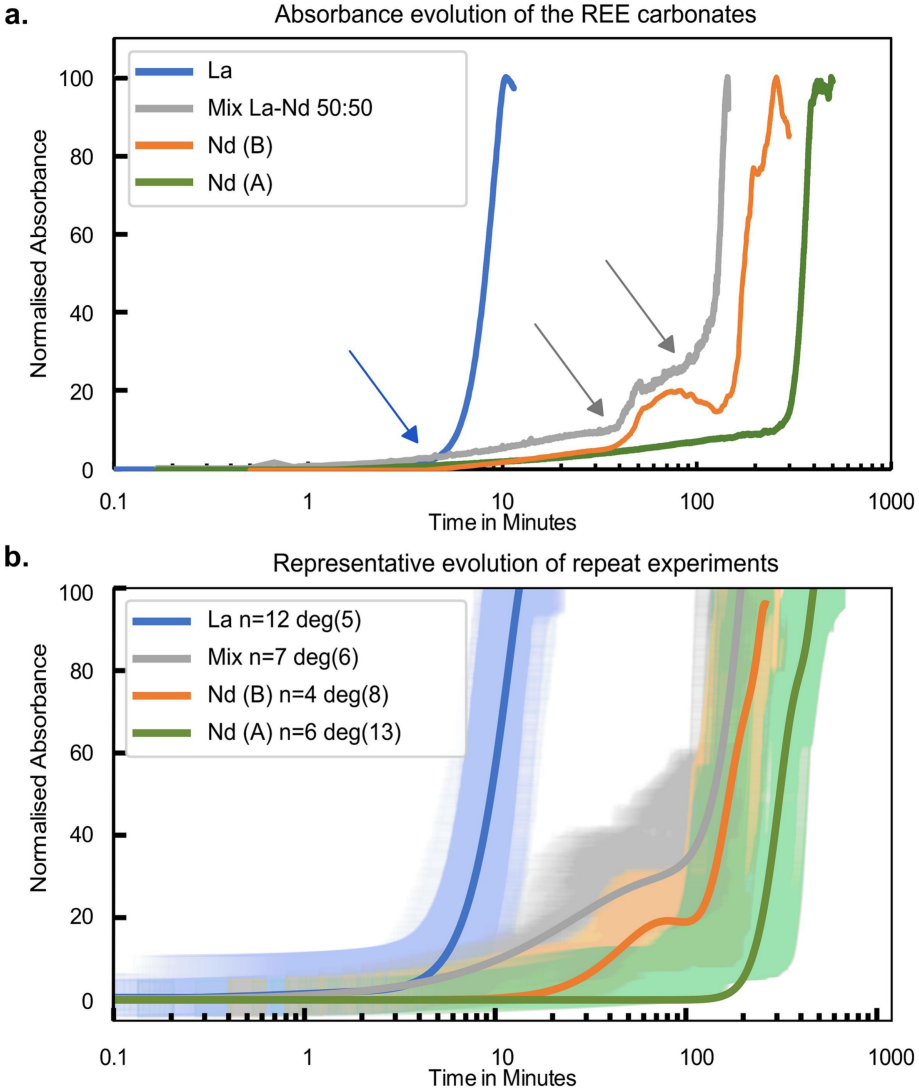
a.
Absorbance evolution of the REE carbonates
La
Mix La-Nd 50:50
Nd (B)
Nd (A)
Normalised Absorbance
Time in Minutes
b.
Representative evolution of repeat experiments
La n=12 deg(5)
Mix n=7 deg(6)
Nd (B) n=4 deg(8)
Nd (A) n=6 deg(13)
Normalised Absorbance
Time in Minutes

Figure 1

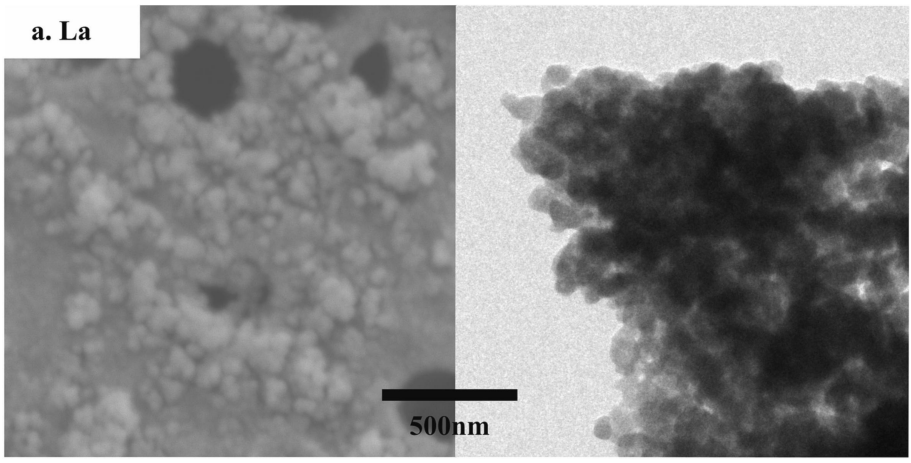
a. La
500nm

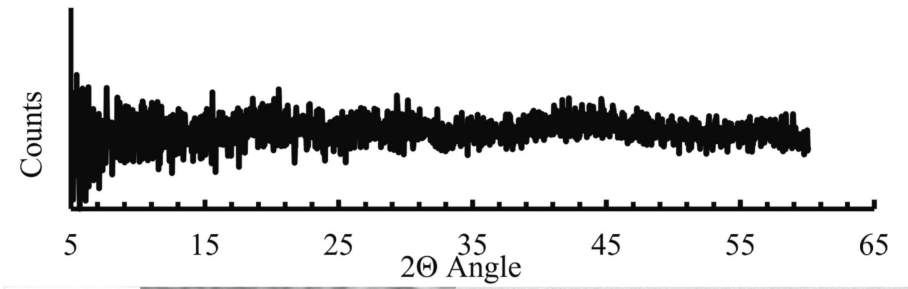
Counts
5
15
25
35
45
55
65
2Θ Angle

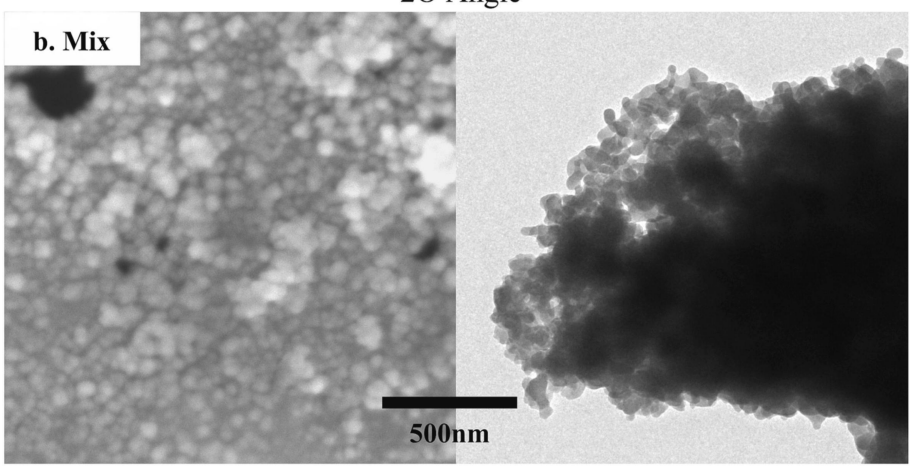
b. Mix
500nm

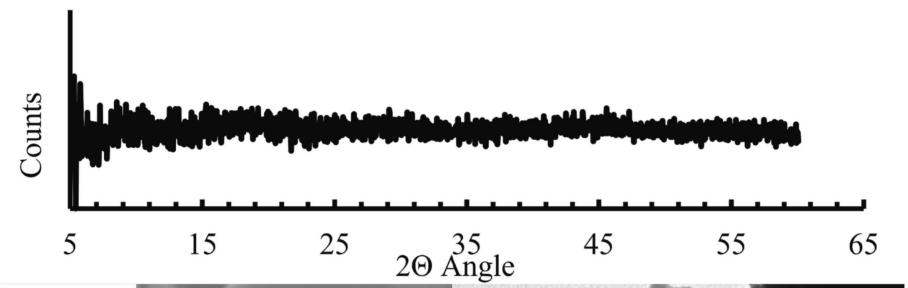
Counts
5
15
25
35
45
55
65
2Θ Angle

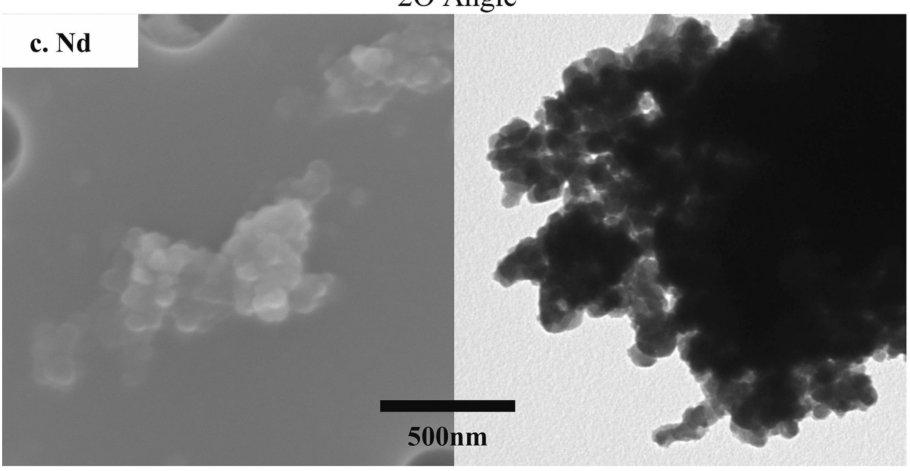
c. Nd
500nm

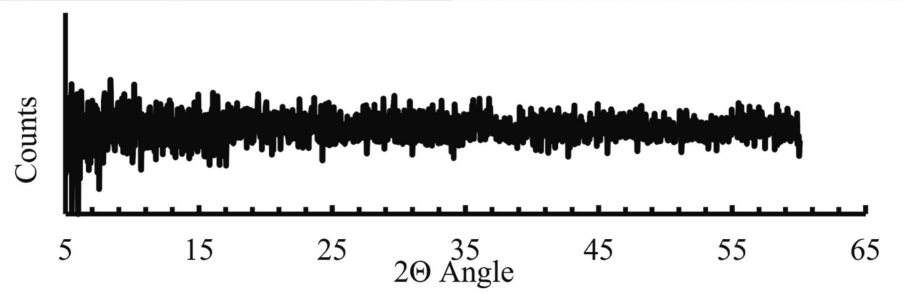
Counts
5
15
25
35
45
55
65
2Θ Angle

Figure 2

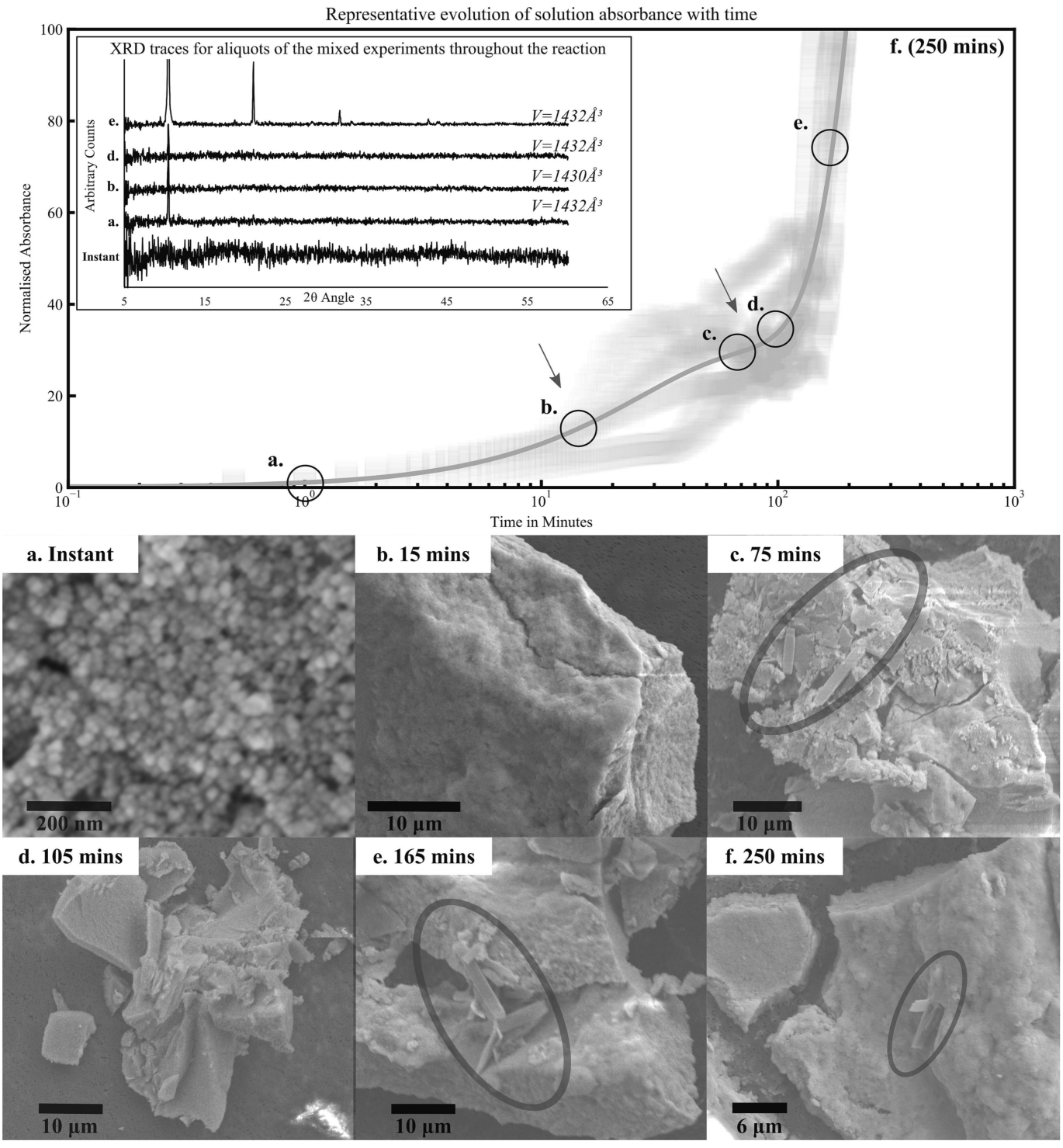
Representative evolution of solution absorbance with time
XRD traces for aliquots of the mixed experiments throughout the reaction
Arbitrary Counts
e.
d.
b.
a.
Instant
V=1432Å³
V=1432Å³
V=1430Å³
V=1432Å³
5
15
25
2θ Angle
35
45
55
65
f. (250 mins)
Normalised Absorbance
Time in Minutes
a.
b.
c.
d.
e.
a. Instant
200 nm
b. 15 mins
10 µm
c. 75 mins
10 µm
d. 105 mins
10 µm
e. 165 mins
10 µm
f. 250 mins
6 µm

Figure 3

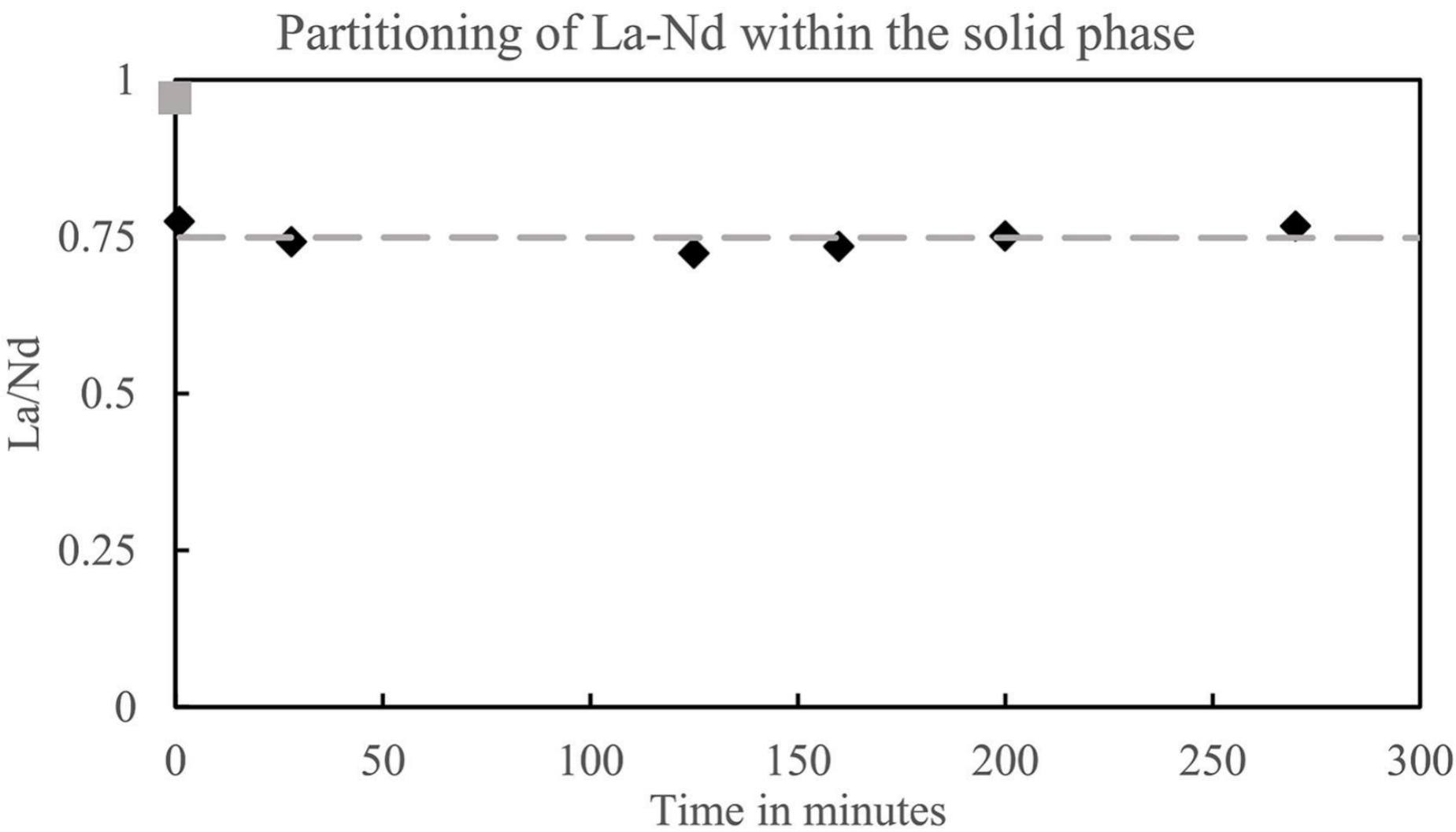
Partitioning of La-Nd within the solid phase
1
0.75
0.5
0.25
0
La/Nd
0
50
100
150
200
250
300
Time in minutes

Figure 4

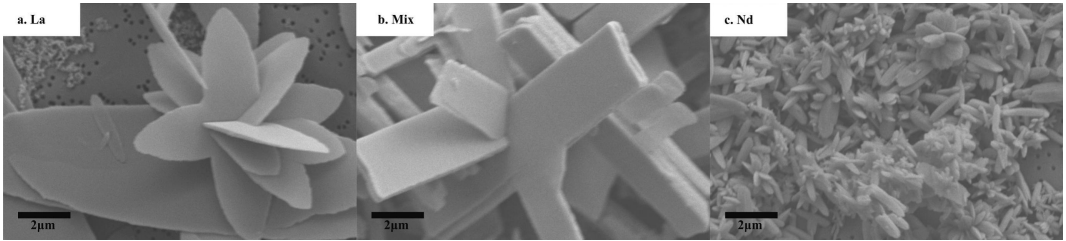

Figure 5

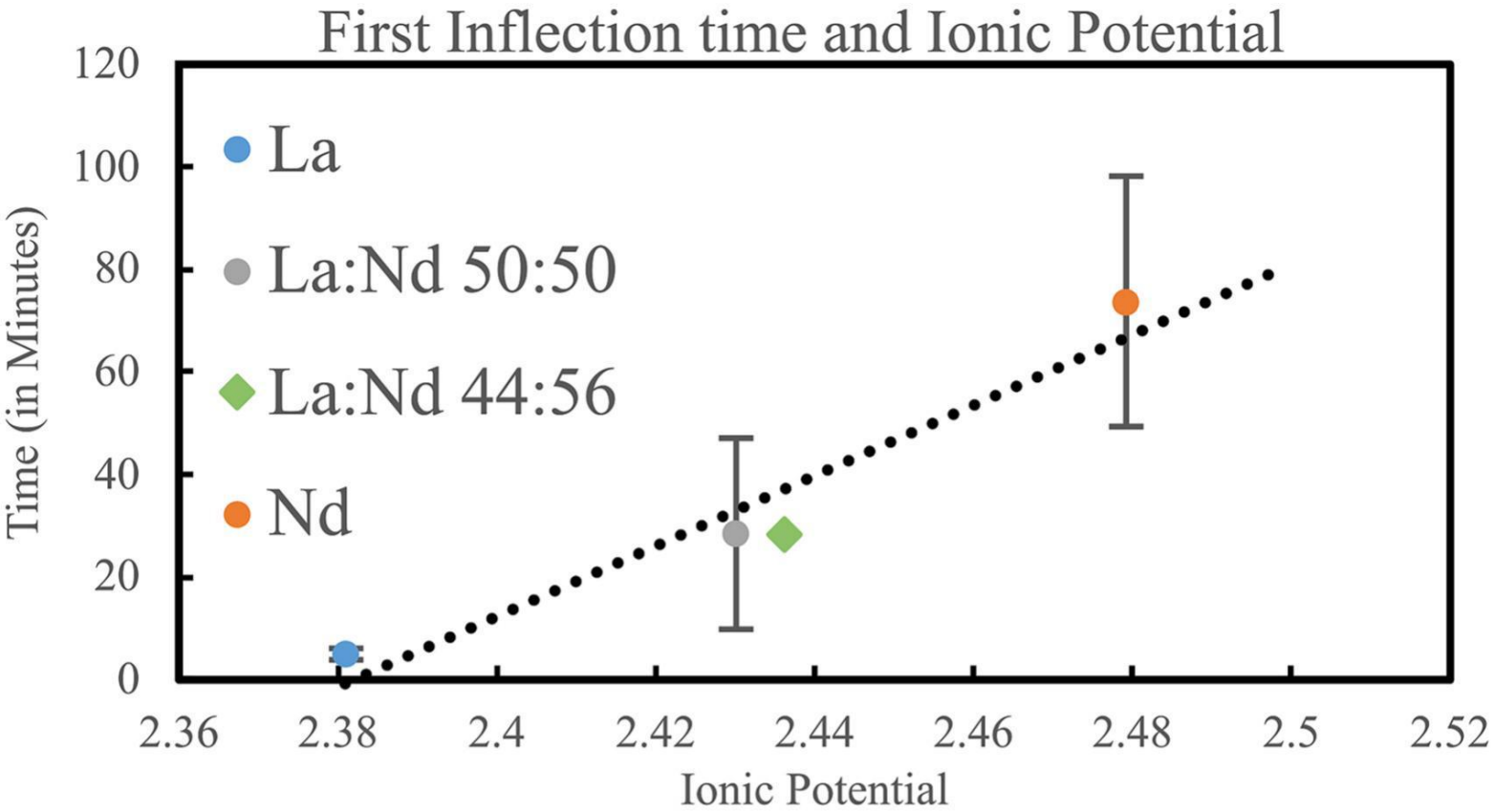
First Inflection time and Ionic Potential
Time (in Minutes)
120
100
80
60
40
20
0
La
La:Nd 50:50
La:Nd 44:56
Nd
2.36
2.38
2.4
2.42
2.44
2.46
2.48
2.5
2.52
Ionic Potential

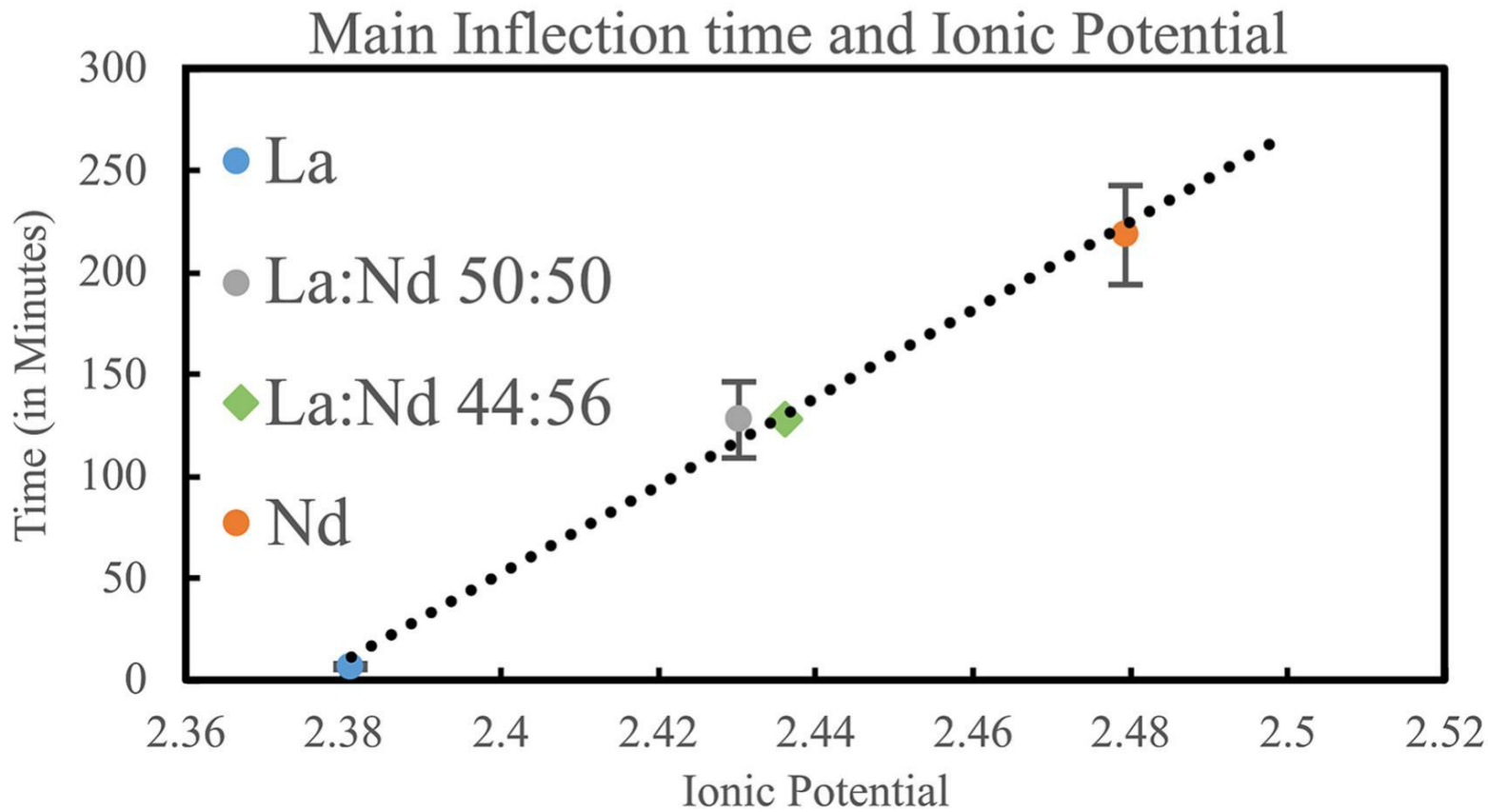
Main Inflection time and Ionic Potential
Time (in Minutes)
300
250
200
150
100
50
0
La
La:Nd 50:50
La:Nd 44:56
Nd
2.36
2.38
2.4
2.42
2.44
2.46
2.48
2.5
2.52
Ionic Potential

Figure 6

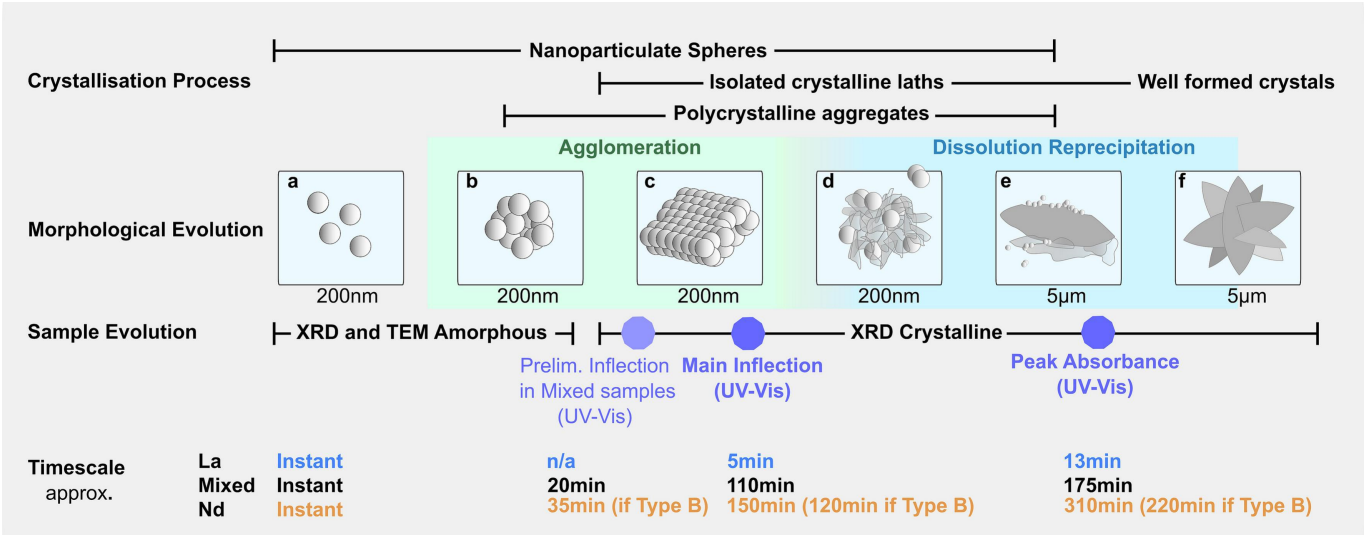
Crystallisation Process
Nanoparticulate Spheres
Isolated crystalline laths
Well formed crystals
Polycrystalline aggregates
Agglomeration
Dissolution Reprecipitation
Morphological Evolution
a
b
c
d
e
f
200nm
200nm
200nm
200nm
5μm
5μm
Sample Evolution
XRD and TEM Amorphous
XRD Crystalline
Prelim. Inflection in Mixed samples (UV-Vis)
Main Inflection (UV-Vis)
Peak Absorbance (UV-Vis)
Timescale approx.
La
Mixed
Nd
Instant
Instant
Instant
n/a
20min
35min (if Type B)
5min
110min
150min (120min if Type B)
13min
175min
310min (220min if Type B)

Figure 7